Received: 2 October 2020 | Revised: 1 September 2021 | Accepted: 12 September 2021

DOI: 10.1111/gcb.15901

Global Change Biology WILEY

PRIMARY RESEARCH ARTICLE

# Regional trends and drivers of the global methane budget

Ann R. Stavert[1,2] | Marielle Saunois[3] | Josep G. Canadell[1,2] | Benjamin Poulter[4] | Robert B. Jackson[5] | Pierre Regnier[6] | Ronny Lauerwald[3,6,7] | Peter A. Raymond[8] | George H. Allen[9] | Prabir K. Patra[10,11] | Peter Bergamaschi[12] | Phillipe Bousquet[3] | Naveen Chandra[13] | Philippe Ciais[3] | Adrian Gustafson[14,15] | Misa Ishizawa[13] | Akihiko Ito[13] | Thomas Kleinen[16] | Shamil Maksyutov[13] | Joe McNorton[17] | Joe R. Melton[18] | Jurek Müller[19] | Yosuke Niwa[13] | Shushi Peng[3] | William J. Riley[20] | Arjo Segers[21] | Hanqin Tian[22] | Aki Tsuruta[23] | Yi Yin[24] | Zhen Zhang[25] | Bo Zheng[3] | Qianlai Zhuang[26]

[1]Global Carbon Project, CSIRO Oceans and Atmosphere, Aspendale, Victoria, Australia

[2]Global Carbon Project, CSIRO Oceans and Atmosphere, Canberra, ACT, Australia

[3]Laboratoire des Sciences du Climat et de l'Environnement, LSCE-IPSL (CEA-CNRS-UVSQ), Université Paris-Saclay, Gif-sur-Yvette, France

[4]NASA Goddard Space Flight Center, Biospheric Science Laboratory, Greenbelt, Maryland, USA

[5]Department of Earth System Science, Woods Institute for the Environment, and Precourt Institute for Energy, Stanford University, Stanford, California, USA

[6]Department of Geoscience, Environment and Society - BGEOSYS, Université Libre de Bruxelles, Brussels, Belgium

[7]Université Paris-Saclay, INRAE, AgroParisTech, UMR ECOSYS, Thiverval-Grignon, France

[8]Yale School of the Environment, Yale University, New Haven, Connecticut, USA

[9]Department of Geography, Texas A&M University, College Station, Texas, USA

[10]Research Institute for Global Change, JAMSTEC, Yokohama, Japan

[11]Center for Environmental Remote Sensing, Chiba University, Chiba, Japan

[12]European Commission Joint Research Centre, Ispra, Italy

[13]Center for Global Environmental Research, National Institute for Environmental Studies (NIES), Tsukuba, Japan

[14]Department of Physical Geography and Ecosystem Science, Lund University, Lund, Sweden

[15]Centre for Environmental and Climate Science, Lund University, Lund, Sweden

[16]Max Planck Institute for Meteorology, Hamburg, Germany

[17]Research Department, European Centre for Medium-Range Weather Forecasts, Reading, UK

[18]Climate Research Division, Environment and Climate Change Canada, Victoria, British Columbia, Canada

[19]Climate and Environmental Physics, Physics Institute and Oeschger Centre for Climate Change Research, University of Bern, Bern, Switzerland

[20]Climate and Ecosystem Sciences Division, Lawrence Berkeley National Laboratory, Berkeley, California, USA

[21]Netherlands Organisation for Applied Scientific Research (TNO), Utrecht, The Netherlands

[22]International Center for Climate and Global Change Research, School of Forestry and Wildlife Sciences, Auburn University, Auburn, Alabama, USA

[23]Finnish Meteorological Institute, Helsinki, Finland

[24]Division of Geophysical and Planetary Science, California Institute of Technology, Pasadena, California, USA

[25]Department of Geographical Sciences, University of Maryland, College Park, Maryland, USA

[26]Department of Earth, Atmospheric, and Planetary Sciences, Purdue University, West Lafayette, Indiana, USA

**Correspondence**
Ann R. Stavert, Global Carbon Project, CSIRO Oceans and Atmosphere, Aspendale, VIC 3195, Australia.
Email: ann.stavert@csiro.au

**Funding information**
Swiss National Science Foundation, Grant/Award Number: #200020_172476; Australian National Environmental Science Program – Earth Systems and Climate Change; Gordon and Betty Moore Foundation, Grant/Award Number: GBMF5439; European Union Horizon 2020, Grant/Award Number: 776810; European Commission, Grant/Award Number: ECMWF CAMS73; Environmental Restoration and Conservation Agency of Japan, Grant/Award Number: JPMEERF20172001 and JPMEERF20182002; US Department of Energy, Grant/Award Number: DE-AC02-05CH11231; European Centre for Medium-Range Weather Forecasts on behalf of the European Commission, Grant/Award Number: CAMS73

## Abstract

The ongoing development of the Global Carbon Project (GCP) global methane ($CH_4$) budget shows a continuation of increasing $CH_4$ emissions and $CH_4$ accumulation in the atmosphere during 2000–2017. Here, we decompose the global budget into 19 regions (18 land and 1 oceanic) and five key source sectors to spatially attribute the observed global trends. A comparison of top-down (TD) (atmospheric and transport model-based) and bottom-up (BU) (inventory- and process model-based) $CH_4$ emission estimates demonstrates robust temporal trends with $CH_4$ emissions increasing in 16 of the 19 regions. Five regions—China, Southeast Asia, USA, South Asia, and Brazil—account for >40% of the global total emissions (their anthropogenic and natural sources together totaling >270 Tg $CH_4$ $yr^{-1}$ in 2008–2017). Two of these regions, China and South Asia, emit predominantly anthropogenic emissions (>75%) and together emit more than 25% of global anthropogenic emissions. China and the Middle East show the largest increases in total emission rates over the 2000 to 2017 period with regional emissions increasing by >20%. In contrast, Europe and Korea and Japan show a steady decline in $CH_4$ emission rates, with total emissions decreasing by ~10% between 2000 and 2017. Coal mining, waste (predominantly solid waste disposal) and livestock (especially enteric fermentation) are dominant drivers of observed emissions increases while declines appear driven by a combination of waste and fossil emission reductions. As such, together these sectors present the greatest risks of further increasing the atmospheric $CH_4$ burden and the greatest opportunities for greenhouse gas abatement.

**KEYWORDS**
anthropogenic emissions, bottom-up, methane emissions, natural emissions, regional, source sectors, top-down

## 1 | INTRODUCTION

Methane ($CH_4$) has a large contribution to the global radiative budget and is responsible for about 0.5°C of present global warming over the period 1850–1900 (IPCC, 2021). Methane has a relatively short perturbation lifetime (12.4 years (Balcombe et al., 2018)) and high global warming potential (28–36 times that of $CO_2$ over a 100-year period (IPCC, 2021)). As such, a decline in $CH_4$ emissions will rapidly reduce global $CH_4$ concentrations and mitigate the impact of climate change at decadal time scales (United Nations Environment Programme & Climate & Clean Air Coalition, 2021). However, any efforts to target $CH_4$ emissions reductions require a thorough understanding of the dominant $CH_4$ sources and sinks and their temporal and regional distribution and trends.

Methane is produced in three ways—pyrogenically, thermogenically, or biogenically—from both anthropogenic and natural processes. Pyrogenic sources of $CH_4$ include biofuel combustion (e.g., wood burning for heating and cooking) and biomass burning (e.g., wildfires and peat fires). All pyrogenic sources produce $CH_4$ from the incomplete combustion of organic matter. Thermogenic $CH_4$ is produced from the breakdown of organic matter buried deep within the Earth's crust at high pressure and temperature. Although geological $CH_4$ is released naturally into the atmosphere through gas seeps, most is released through activities related to the exploration, mining, and transport of fossil fuels (Hmiel et al., 2020; Janssens-Maenhout et al., 2019; Petrenko et al., 2017). The majority of biogenic $CH_4$ is produced in anaerobic environments by the microbial mediated breakdown of organic matter. These environments include wetlands, inland waters, marine sediments, ruminants such as cattle, rice paddies, manure management and wastewater and landfill systems. Small quantities of $CH_4$ are also produced from the aerobic bacterial metabolization of methylated compounds (e.g., Florez-Leiva et al., 2013) and even photochemically (Li et al., 2020).

Counter-balancing these $CH_4$ sources are three chemically driven atmospheric sinks of $CH_4$. The first two reactions with tropospheric OH radicals and tropospheric atomic chlorine account for ~88% (476 – 677 Tg $CH_4$ $yr^{-1}$) and ~2% (1–35 Tg $CH_4$ $yr^{-1}$) of the total sink, respectively, with a third stratospheric sink (e.g., reaction with O('D), Cl and OH in the stratosphere) accounting for a further ~5% (12–37 Tg $CH_4$ $yr^{-1}$) (Saunois et al., 2020). However, due to their highly reactive nature, the key reactants are inherently difficult to quantify, driving a significant level of uncertainty in the spatial and temporal distribution of atmospheric sink estimates (Zhao et al., 2019). Many fundamental aspects of the spatial distribution of OH are currently unresolved, for example, estimates of the interhemispheric gradient can vary from 0.85 to 1.4 (NH/SH) depending on the methodology

(See Patra et al., 2014 and references therein). The large-scale geographical breadth of many of the chemical and physical drivers in OH spatial variability associated with intra- and interhemispheric transport of $CH_4$ over 1 year (Anderson et al., 2021) make the OH sink incompatible with a geo-politically defined surface-region-based study (the focus of this paper). As a result, only sources of $CH_4$ are discussed at regional scale in this study.

A fourth sink is the biological consumption of $CH_4$ by methanotrophic microbes in soils and other environments. It is estimated to be responsible for 5% of the global total $CH_4$ sink (Saunois et al., 2020). This process occurs in aerobic soils and inland waters where methanotrophic bacteria consume $CH_4$ and produce $CO_2$ (Le Mer & Roger, 2001). The oxidation of $CH_4$ can occur at the same site as the production of $CH_4$ either concurrently (e.g., aerobic soils capping landfills) or temporally shifted (e.g., sediments shifting from anoxic to oxic with seasonal waterflow patterns). As such, the oxidative process can play a role in controlling $CH_4$ emissions to the atmosphere. In this paper, rather than separating production and consumption we focus on the policy relevant net surface emissions and exclude discussion of some spatially diffuse non-anthropogenic fluxes (e.g., upland soil sinks).

This paper analyzes the recently published global $CH_4$ budget Saunois et al. (2020) and conducts an in-depth examination of $CH_4$ (total and sectoral) emission trends in 19 regions. Here we examine regions defined using geo-political boundaries and focus on net surface emissions (rather than separating production and consumption) because they are more directly relevant to policy analyses and the development of effective regional mitigation strategies. We use, as in Saunois et al., 2020, multiple emissions estimates from top-down (TD) approaches, based on atmospheric constraints, and bottom-up (BU) methods, which use extensive data inventories, terrestrial biospheric modelling, and the statistical upscaling of empirical data.

In presenting data from a range of BU and TD methods this paper reflects the current state of science in relation to global-scale estimates of regional $CH_4$ emissions. By also clearly and concisely articulating their current limitations we build the groundwork for future research which will incorporate improvements in TD and BU methodologies. Using multiple methodologies allows us to estimate not only the uncertainty of these regional emissions (using the spread in emissions estimates) but also the uncertainty in the regional trends (using the spread in emissions trends). Although not totally independent of BU methods (see Section 2.2), TD methods rely on $CH_4$ atmospheric mole fraction measurements which are an independent observational constraint. As such, commonalities between multiple BU and TD estimates can identify robust trends and patterns in regional $CH_4$ emissions and differences suggest areas requiring further investigation.

A regional decomposition (rather than latitudinal as in Saunois et al. (2020)) is essential as the drivers of $CH_4$ emissions vary widely in their spatial distribution and relative importance with climate, ecosystem type, anthropogenic activities and environmental policies. We also examine both decadal and annual data for the 2000–2017 period allowing the identification of trends and policy impacts.

Here, we aggregate $CH_4$ emission types into five (three anthropogenic and two natural) key source sectors: agriculture and waste (*Ag&Waste*), fossil fuel (*Fossil*), biomass burning and biofuels (*BB&F*), wetlands (*Wetl*), and other natural non-wetland (*NonWetl*).

We then examine four key questions pertinent to the design and implementation of emission reduction strategies:

1. Which regions are the largest contributors to global $CH_4$ emissions?
2. Which activities or sources are driving these emissions?—natural vs. anthropogenic sources and specific source sector types.
3. Which regions are the dominant contributors to the increasing trend in global $CH_4$ emissions and which sectors are driving this rise?
4. Are any regions seeing a decline in $CH_4$ emissions and which sectors are responsible for this decline?

We also examine the key differences in TD and BU estimates, using them to identify methodological limitations and to highlight uncertainties and areas requiring further investigation.

## 2 | METHODS AND MATERIALS

The spatial distribution of sources and sinks of $CH_4$ can be quantified using TD or BU approaches. BU approaches include process-based models, inventories, satellite-based products, and other data sets, which collate and scale-up local (or regional) direct flux measurements (e.g., flux towers and chamber-based approaches). Most commonly, BU-based estimates of anthropogenic $CH_4$ emissions are determined using inventory methods (e.g., EDGAR v4.3.2, Janssens-Maenhout et al., 2019). Here, known regionally distributed activity information and statistics are combined with technology-specific emission factors and abatement factors which account for recapture and emissions mitigation technology. Satellite-derived biomass burning products combine estimates of the area burned, biomass loading, combustion completeness and biome-specific emission factors to estimate $CH_4$ emissions (e.g., van der Werf et al. (2017)). Process-based models, for example wetland models (e.g., Poulter et al. (2017)), can also be used to estimate sector-specific regionally distributed $CH_4$ emissions. Lastly, a variety of methods have been used to statistically scale up small-scale or sparse empirical measurements of $CH_4$ flux to regional and global totals (e.g., Etiope et al., 2019). Regional studies, which typically use region specific data sets and methodologies, are not included in this analysis as they may bias cross-region comparisons. Instead, where appropriate, regional studies are used to inform the discussion of trends identified in the global-scale regionally distributed data sets.

TD approaches take observed atmospheric mole fractions of $CH_4$ and combine them with global (or regional) transport models and an inversion framework to calculate an optimum set of spatially and temporally distributed source and sink fluxes. Studies using this approach are plentiful and use a variety of transport models, inversion methods, atmospheric data sets (in situ, flask, total column ground-based and satellite) and prior flux estimates. Examples

include Bergamaschi et al. (2018), Maasakkers et al. (2019) and Yin et al. (2021). Some methods aim to separate certain emission sectors based on differences in their spatial and temporal distributions (e.g., Bergamaschi et al. (2013)), while others only solve for net emissions at the surface (Chandra et al., 2021). Then the partitioning of TD posterior (output) fluxes between specific source sectors (e.g., *Fossil* vs. *BB&F*) is carried out with various degrees of uncertainty depending on the methods and the degree of refinement of sectors.

Here, we use a subset of the ensemble of TD and BU data sets gathered in Saunois et al. (2020) (see Section 2.1 and 3.2.1) and a newly developed inland water emissions estimate (see Section 2.1.4 and S2). This approach means that the sum of the regional (and sectoral) budgets presented here, while very similar, are not equivalent to the global budget presented in Saunois et al. (2020) (see Section 3.2.1).

## 2.1 | Bottom-up data

### 2.1.1 | Anthropogenic

A summary of the key global anthropogenic BU assessments used in this paper is given in Table 1, with further details found in Saunois et al. (2020) and the references therein. Here, we focus on the four global gridded anthropogenic data sets that encompass the sectors of interest, namely EDGAR v4.3.2. (Janssens-Maenhout et al., 2019), GAINS ECLIPSE v6 (Höglund-Isaksson et al., 2020), USEPA, 2012 (USEPA, 2012) and CEDS (Hoesly et al., 2018). For ease of reading, these will henceforth be referred to as EDGAR, GAINS, USEPA, and CEDS. It is important to note that while included in the analysis, the CEDS inventory (Hoesly et al., 2018) is based partly on an earlier data set (EDGARv4.2) which is known to overestimate Chinese coal emissions (Peng et al., 2016). As FAO does not provide *Waste*, *Fossil* and *Biofuel* emission estimates we, unlike Saunois et al. (2020), do not include these in our analysis.

### 2.1.2 | Biomass burning

Six biomass burning emissions estimates—FAO (FAO, 2019b), FINNv1.5 (Wiedinmyer et al., 2011), GFASv1.3 (Kaiser et al., 2012), GFEDv4.1s (van der Werf et al., 2017), QFEDv2.5r1 (Darmenov, 2015) and the USEPA emissions inventory (USEPA, 2012)—were discussed in Saunois et al. (2020). The FAO data (FAO, 2021) were updated in December 2020 after the publication of Saunois et al. (2020) and both the original and updated versions are included in Figure S1. Key differences among biomass burning estimates include the lack of interannual variability (IAV) in the USEPA estimate and the unusually high (by a factor of 2–10, e.g., Figure S1 USA and Russia) regional emissions of the original FAO estimates. Here, unlike Saunois et al. (2020), we use the mean of the updated FAO (FAO, 2019b), FINNv1.5 (Wiedinmyer et al., 2011), GFASv1.3 (Kaiser et al., 2012), GFEDv4.1s (van der Werf et al., 2017), and QFEDv2.5r1 (Darmenov, 2015) estimates of biomass burning.

### 2.1.3 | Wetlands

Regional BU *Wetl* estimates were examined using 13 models from the wetland model intercomparison conducted as part of the 2020 GCP $CH_4$ budget project (GCP, 2021). These model runs use a common wetland extent map (diagnostic) (Zhang et al., 2021) while nine prognostic runs (which were not used for regional estimates but do inform the discussion) used a range of internally generated wetland extent maps (see supplement Section 4 of Saunois et al. (2020)). Mean regional BU *Wetl* estimates were calculated using the data from the diagnostic wetland model runs.

### 2.1.4 | Non-wetland sources including oceanic

Four BU estimates of total other natural non-wetland (*NonWetl*) sources were calculated in this study. They ranged between 177–186 Tg $CH_4$ $yr^{-1}$ and were determined as the sum of the three main sources: aquatic biogenic (including inland waters, oceanic, estuaries and blue carbon, i.e., mangroves, seagrasses and marsh systems), geological (land and ocean), and termite.

Here, we use a new estimate of global inland water and estuarine fluxes (Section S2). It is the first global-scale regionally distributed data set of this nature and was calculated as the sum of lake and reservoir, river and stream and estuarine fluxes. It was developed specifically for this study and not available at the time of publication for Saunois et al. (2020).

The biogenic oceanic estimate calculated by Saunois et al. (2020), 6 Tg $CH_4 yr^{-1}$ (range 4–10 Tg $CH_4$ $yr^{-1}$), included oceanic, estuarine and blue carbon fluxes. But estuarine and blue carbon fluxes occur at the interface between land and marine waters (i.e., straddling both land and ocean regions). In this study we treat the global oceans as a single region, hence to spatially distribute the estuarine and blue carbon fluxes they have been allocated to the adjacent land, rather than the ocean region. As such, the ocean biogenic component used in this study (3 Tg $CH_4$ $yr^{-1}$) was calculated as the difference between the Saunois et al. (2020) total oceanic biogenic flux (6 Tg $CH_4$ $yr^{-1}$) and the total of the new independent regionally distributed estimate of estuarine flux (3 Tg $CH_4$ $yr^{-1}$).

Only a single spatially distributed estimate of geological $CH_4$ emissions, 37 Tg $CH_4$ $yr^{-1}$, is available (Etiope et al., 2019). This estimate is lower than the mean global total reported by Saunois et al. (2020) but well within their range, 18–65 Tg $CH_4$ $yr^{-1}$. Termite emissions are based on four distributions (one each from Kirschke et al. (2013); Saunois et al. (2016) and two from Saunois et al. (2020)) and range between 9 and 18 Tg $CH_4$ $yr^{-1}$.

It is important to note that although these four sectors represent the four largest natural non-wetland $CH_4$ emissions, other natural flux types, such as wild animals, are excluded as their regional

**TABLE 1** Components of the total bottom-up emission estimates and references

| Sector abbreviation | Subsector | Information type | Bottom-up estimate | | | |
|---|---|---|---|---|---|---|
| | | | **CEDS** | **EDGAR** | **GAINS** | **USEPA** |
| Fossil | Total Fossil | Temporally and spatially varying | CEDS (Hoesly et al., 2018) | EDGAR v4.3.2 (Janssens-Maenhout et al., 2019) | GAINS ECPLISE v6 (Höglund-Isaksson et al., 2020) | USEPA (USEPA, 2012) |
| Ag&Waste | Agriculture and waste | | | | | |
| BB&F | Biofuels | | | | | |
| | Biomass Burning | | BB4CMIP (van Marle et al., 2017) | | GFEDv4.1s (van der Werf et al., 2017) | |
| Wetl | Wetlands | | Ensemble mean of wetlands models (Saunois et al., 2020; Zhang et al., 2021) | | | |
| Non-Wetl | Geological | Spatially but not temporally varying | Etiope et al. (2019) | | | |
| | Termites | | Kirschke et al. (2013), Saunois et al. (2016) and Saunois et al. (2020) | | | |
| | Oceanic (biogenic) including estuaries and blue carbon | | Ocean total of 6 Tg $CH_4$ $yr^{-1}$ as described in Saunois et al. (2020) | | | |
| | Inland waters – lakes and reservoirs* | | This paper Section 2.1.4 and Supplementary S4. | | | |
| | Wild animals | Global totals only | Excluded from total | | | |
| | Permafrost soils | | | | | |

*The inland water estimate was developed for this study and was not used in Saunois et al. (2020).

distribution was either unknown or poorly characterized. Global estimates of these omitted fluxes are very small, ranging between 1 and 4 Tg $CH_4$ $yr^{-1}$, <0.6% of total emissions (Saunois et al., 2020). Considering the magnitude of the uncertainties in the inland waters, oceanic, and termite estimates (>100%), it is expected that this omission is easily encompassed in the inherent uncertainty of the *NonWetl* estimates.

## 2.2 | Top-down data

As described in Saunois et al. (2020, Section 4.2) a comparison of nine different inversions systems together resulting in a total of 22 inversion simulations was conducted. A set of common prior source and sink estimates were developed and these, along with a set of atmospheric observations (Figure 1), were provided to the participants (Saunois et al., 2020, Supplementary material). However, their use was not compulsory (See Saunois et al. (2020) Table S6 for further information). Monthly gridded prior and posterior flux estimates for each of the five broad subsectors were submitted by participants for analysis at 1°× 1° grid resolution. Further details including the theory of atmospheric inversions, the models and the atmospheric observations used in our study can be found in Saunois et al. (2020).

There are three key details to note with TD inversions. Firstly, they fit to the observed atmospheric $CH_4$ mole fraction (i.e., the difference between $CH_4$ sources and sinks) rather than directly fitting to the individual sources or sinks. As part of this process all but two inverse models (TOMCAT and PYVARLMDz, Table S1) used a spatially varying but 12-month climatological prior estimate of the global $CH_4$ sink. This assumption is a significant limitation as this sink can vary interannually (Zhao et al., 2019). As such, for TD methods, some temporal variability in the chemical sink may instead be assigned to temporal variability in the source estimates. Similarly, variability in the spatial distribution of the chemical sink may also drive variability in the spatial distribution of the TD-derived regional $CH_4$ sources. However, as five estimates of the chemical sink spatial distribution were used in our suite of inversions this source of uncertainty should be reflected in the spread of the ensemble of the inversions.

Secondly, rather than optimizing for individual source sectors (e.g., *Fossil* or *Wetl* fluxes) some inversions optimize for the total flux for each region or pixel and then partition it to source sectors using a fixed regional ratio of sources calculated from prior flux information at pixel scale. This partitioning can lead to significant uncertainties if not all sources increase or change at the same rate in a given region or pixel. However, optimizing by pixel rather than region does allow finer spatial scale adjustments which may reduce any aggregation errors. Similarly, uncertainties in the priors can drive uncertainties in the sectoral emissions estimates of systems, which optimize for individual sectors as, when relying on $CH_4$ observations alone (as opposed to the use of $CH_4$, $CH_4$ isotopes, and related tracers), it is the spatio-temporal distribution of the priors, which drives the sectoral differentiation. Here, seven of the nine inversion systems optimize for some source sectors (that can differ from our sectors) and the other two (MIRO4-ACTM and PYVARLMDz) solve for net total emissions (Table S1). Thirdly, TD methods generally use BU estimates as prior knowledge and as such BU and TD methods cannot be considered as truly independent.

## 2.3 | Data processing

Data sets were provided on a variety of grids, at different temporal resolutions and over a range of time periods (Supplementary Section S1 and references within Table 1). These data sets were regridded, projected to a common grid and interpolated or extended to a common temporal resolution and time period (Supplementary Section

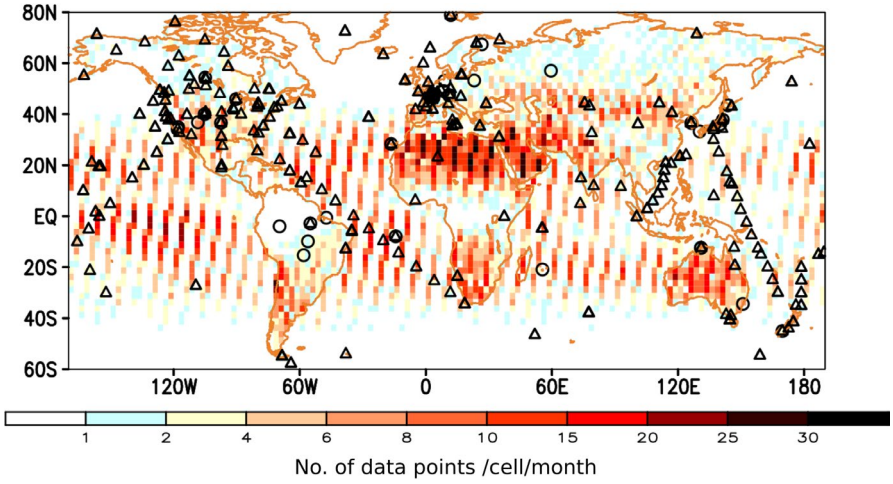


FIGURE 1 The locations of the surface (triangle) and ground-based profile (circle) observation sites and GOSAT $XCH_4$ data density and extent (number of data points per grid cell per month for NIES full physics retrievals) for 2014. Grid cells are 2.5 × 2.5°. Note that many of the in situ sites are not operational or are not reporting data to the Global Atmospheric Watch repository. Also note that many of the GOSAT grids do not have uniform data coverage in all months as the instrument cannot see through the cloud covered areas and during polar nights

S1). Regions (18 land and 1 ocean) were constructed using geopolitical boundaries and chosen on the basis of size, geopolitical importance, and vegetation type (Figure 4 and Saunois et al. (2020) Table S1). Box plots of emissions estimates were calculated for the period 2008–2017 (Supplementary Section S3). Rates of change in regional and global emissions estimates were calculated over the 2000–2017 period as described in the Supplementary (Section S4). Comparisons of TD and BU regional emissions were made for the total regional $CH_4$ emission, the total natural and total anthropogenic emissions and sectoral emissions.

#### 2.3.1 | Sector definitions

Methane emission types were aggregated into five key source sectors (see also Supplementary S5):

1. Agriculture and waste (*Ag&Waste*)—net emissions related to agriculture, including rice cultivation and ruminant farming, and waste management activities, except agricultural waste burning
2. Fossil fuel (*Fossil*)—emissions related to fossil fuel exploration, extraction, transport, distribution, production and use, including fugitive and industrial emissions
3. Biomass burning and biofuels (*BB&F*)—emissions related to biomass burning (including agricultural waste burning) and biofuel usage
4. Wetlands (*WetI*)—Net wetland emissions
5. Other natural non-wetlands (*NonWetI*)—The sum of net inland water, net oceanic, geological (land and ocean), and termite emissions

#### 2.3.2 | Bottom-up estimates—total anthropogenic and natural

Total BU anthropogenic emissions were calculated as the sum of the *Fossil*, *BB&F*, and *Ag&Waste* emissions for each of the emissions inventories. Five BU total anthropogenic emissions estimates were calculated, one for each of the four major anthropogenic emissions inventories and a mean of the four. Total BU natural emissions were calculated as the sum of the mean *NonWetI* emissions estimate and each of the 13 wetland process-based models using the diagnostic wetland area resulting in 13 estimates of total natural emissions.

In an effort to reduce the number of BU total emissions estimates, the mean of the *NonWetI* estimate (i.e. the sum of inland waters, termites, oceans, and geological fluxes) and the mean *WetI* flux were combined with the five anthropogenic estimates to produce five BU estimates of total emissions. However, comparisons between the TD and BU estimates of *WetI* fluxes were made using the full suite of 13 BU estimates and the mean. Similarly, TD and BU comparisons of *NonWetI* fluxes were made using five BU estimates (one for each termite estimate) and the mean.

#### 2.3.3 | Top-down estimates

A total of 22 different gridded TD total source estimates were provided from the nine inversion systems included in Saunois et al. (2020). Of these, half were based solely on surface $CH_4$ data (TD SURF) and half included GOSAT satellite data (TD GOSAT). Separate TD SURF and TD GOSAT annual and decadal means were calculated globally and for each region. Unlike Saunois et al. (2020), here the decadal mean, median, and box plot calculations are based only on the SURF data. In some cases, multiple simulations were provided for a given inversion system. To avoid overweighting these inversion systems, the mean of each inversion system's simulations, rather than each individual simulation, was used to calculate the mean timeseries. However, to demonstrate the spread in the TD estimates the individual simulations were included in the time series figures. See Table S2 for further information.

Total TD anthropogenic emissions were calculated separately for each inversion simulation as the sum of the *Fossil*, *BB&F*, and *Ag&Waste* emissions. Similarly, total TD natural emissions were calculated separately for each inversion simulation as the sum of the *NonWetI* (including ocean emissions) and *WetI* emissions.

## 3 | RESULTS

We first focus on commonalities between the BU and TD estimates, identifying robust features in the spatial distribution and temporal trends of $CH_4$ emissions with the aim of addressing the four key questions outlined earlier (Section 3.1). Second, we highlight key TD and BU differences (Section 3.2).

In the text we report median BU values along with their 25th to 75th percentile range as median [25th-75th percentile] Tg $CH_4$ $yr^{-1}$ with the equivalent measures for TD estimates following in parentheses. This reporting approach differs from Saunois et al. (2020), who reported the mean and min-max range. Similarly, when discussing BU and TD estimates as a percentage or changes in emissions rates we report the BU value and give the TD value in parentheses, i.e., BU (TD).

For consistency and completeness when discussing sectoral $CH_4$ emissions we report both the BU and TD values. However, it is important to note that TD sectoral estimates are dependent on BU estimates and due to the methodology used, there are significant uncertainties associated with the TD sectoral estimates (Section 2.2).

### 3.1 | Bottom-up and top-down commonalities, trends, and regional hotspots

#### 3.1.1 | Total $CH_4$ emissions

Mean global total $CH_4$ emissions for 2008–2017 are estimated to be BU = 689 [25th-75th percentile = 677–697] (TD = 572 [568–581])

Tg $CH_4$ $yr^{-1}$. TD and BU regional total emissions for the most recent decade (2008–2017) are shown in Figure 2. Five regions dominate total emissions: China, Southeast Asia, USA, South Asia, and Brazil. Together these five regions account for BU = 43% (TD = 49%) of total global $CH_4$ emissions, with 298 [279–312] (273 [256–305]) Tg $CH_4$ $yr^{-1}$ in the 2008–2017 decade. Comparisons of the 2000–2009, 2003–2012, and 2008–2017 decadal means show these regional rankings to be fairly consistent over time (Table S3). Information in relation to latitudinal flux distribution can be found in Table 5 of Saunois et al. (2020).

### 3.1.2 | Anthropogenic and natural $CH_4$ emissions

Natural emissions are dominated by five regions—Brazil, Canada, Equatorial Africa, Russia, and Southeast Asia (Figure 3). Together these five regions produce BU = 48% (TD = 52%) of the global natural emissions, with BU = 158 [133–181] (TD = 104 [95–121]) Tg $CH_4$ $yr^{-1}$ (Figure 3). In comparison, regional anthropogenic emissions can be divided into three groups, those >40 Tg $CH_4$ $yr^{-1}$, those 20 to 40 Tg $CH_4$ $yr^{-1}$ and those <20 Tg $CH_4$ $yr^{-1}$ (Figure 3 and Figure S2a). The two regions in the first group, China, 59 [50–68] (45 [41–55]) Tg $CH_4$ $yr^{-1}$, and South Asia, 45 [41–47] (46 [43–49]) Tg $CH_4$ $yr^{-1}$, together account for 29% (26%) of global anthropogenic emissions. The second group of regions, which together account for 55% (56%) of anthropogenic emissions, include the USA, Brazil, Europe, Northern and Equatorial Africa, Russia, the Middle East, and Southeast Asia, each emitting between 20 and 40 Tg $CH_4$ $yr^{-1}$. The rest of the world (nine regions) emit ≤10 Tg $CH_4$ $yr^{-1}$ per region. Median anthropogenic per capita emissions for 2008 to 2017 (Figure S2d) range from a low of 0.02 Tg $CH_4$ $yr^{-1}$ million $people^{-1}$ (Korea and Japan) to a high of 0.2 Tg $CH_4$ $yr^{-1}$ million $people^{-1}$ (Oceania).

The fraction of regional anthropogenic emissions can differ between TD and BU estimates, with only 8 of the 19 regions agreeing within the 25th-75th percentile range (Figure 3c). However, the relative region-to-region pattern has some similarities with the methods having the five lowest regions in common – namely Canada, Oceans, Southwest South America, Brazil, and Northwest South America. Similarly, Europe, Korea and Japan, Middle East, South Asia, and China are common to both the TD and BU top six regions when ranked by anthropogenic proportion. Some regions, including China, the Middle East, and South Asia, are dominated by anthropogenic emissions (BU and TD >75% of total emissions), whereas in other regions (e.g., Canada) most emissions come from natural sources (> 70%) (Figure 3c).

### 3.1.3 | Sectoral $CH_4$ emissions

The sectoral breakdowns for each of the five global hotspot regions—USA, China, South Asia, Southeast Asia, and Brazil—show distinct patterns (Figure 4). The majority of Chinese emissions

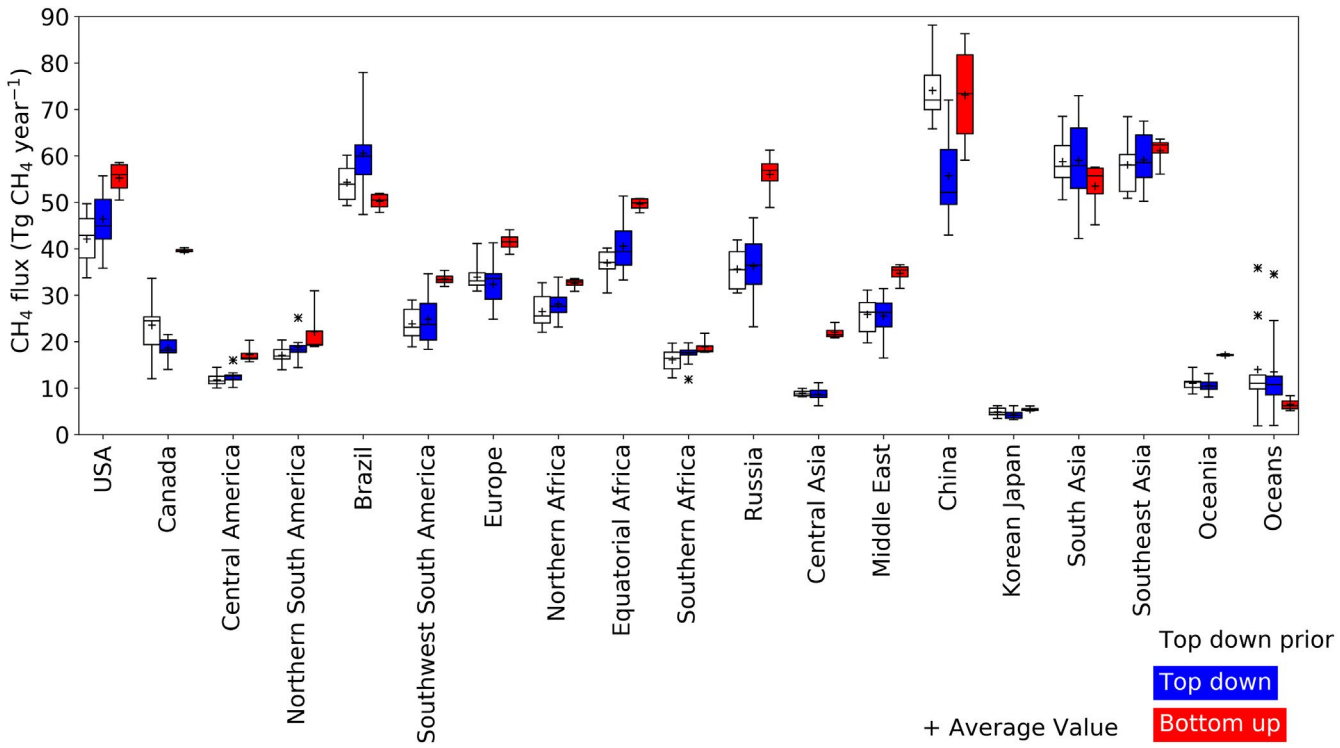


FIGURE 2 Boxplots of the total source estimates for the most recent decade (2008–2017) for each region for the bottom-up (BU—red boxes) and top-down surface sites only (TD SURF—blue boxes). The priors used in the TD SURF estimate are also shown (empty boxes). The box represents the 25th to 75th percentile range, "x" represents the outliers and the whiskers show the minimum and maximum values (outliers excluded)

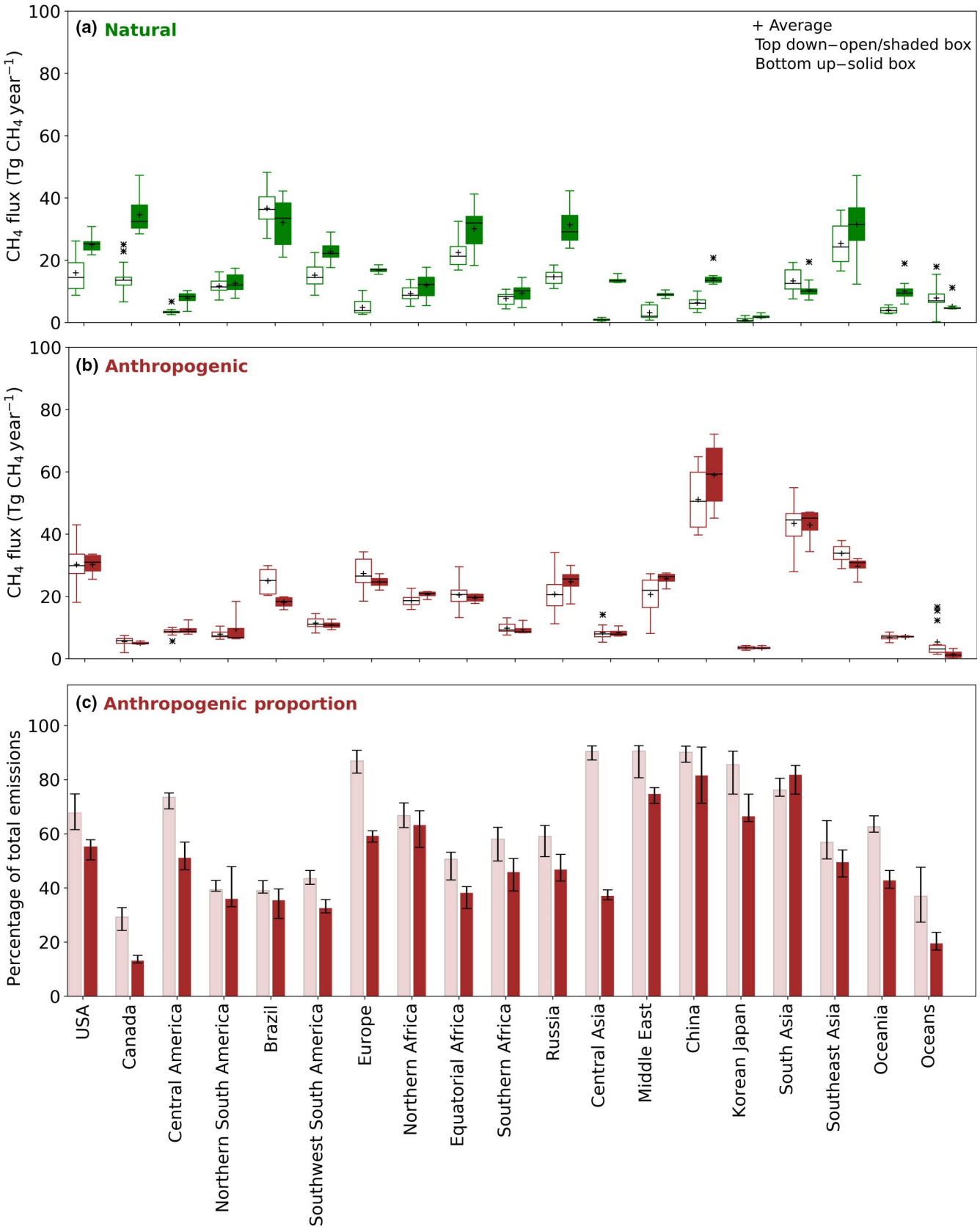


FIGURE 3 (a) Natural (green) emissions by region, (b) mean anthropogenic (brown), and (c) mean anthropogenic proportion as a percentage of total regional emissions (brown) in Tg $CH_4$ $yr^{-1}$ for 2008–2017. Bottom-up (BU) estimates are shown as filled boxes and top-down surface sites only (TD SURF) as open boxes. The box represents the 25th to 75th percentile range, "x" represents the outliers and the whiskers show the minimum and maximum values (outliers excluded)

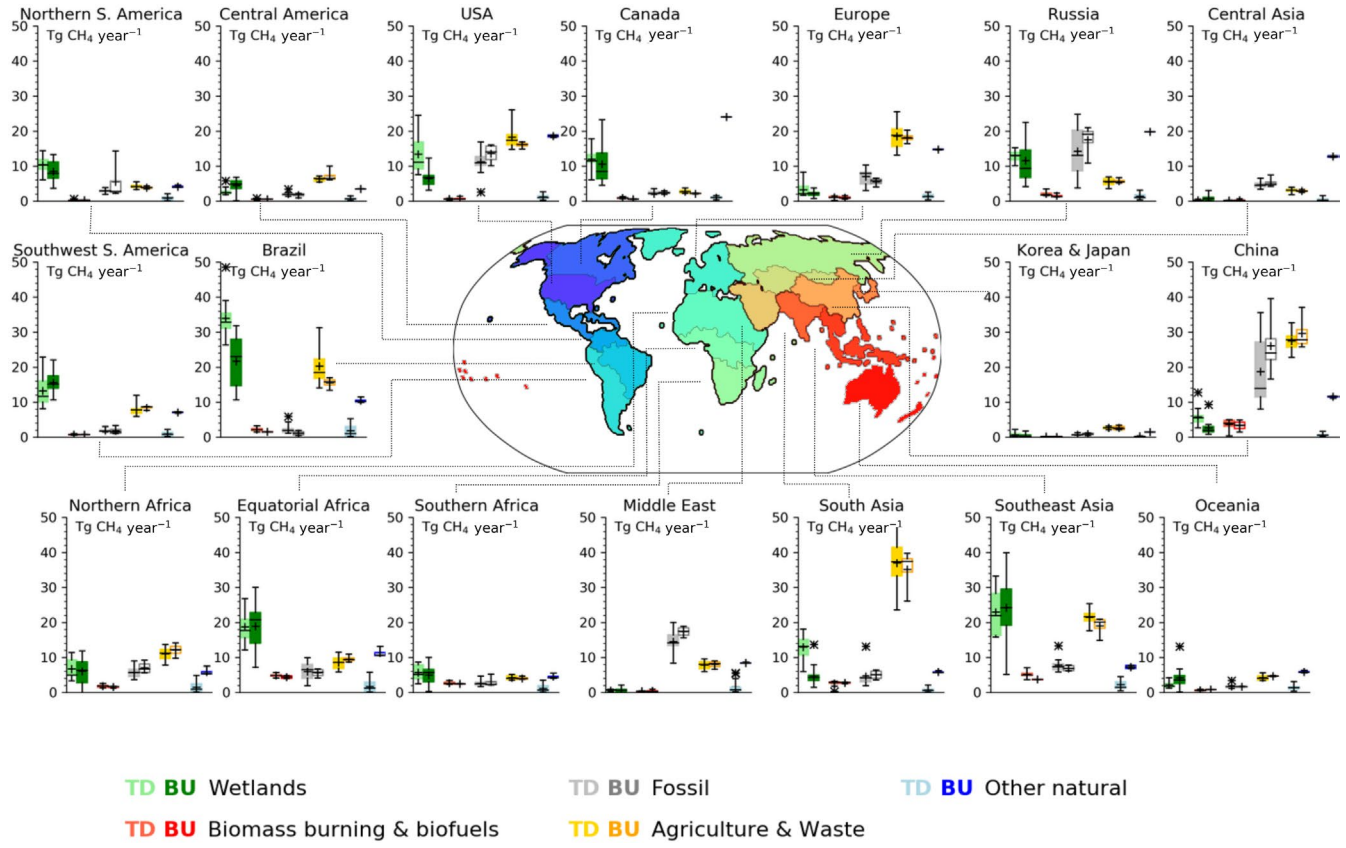


**FIGURE 4** The sectorial budget breakdown for each region in Tg $CH_4$ $yr^{-1}$ for the most recent decade (2008–2017) and a map of the 18 land regions used in this study. Each panel shows methane emissions for the five key sectors, from left to right: Wetlands, Biomass burning and biofuels, Fossil fuels, Agriculture & waste, and Other natural (including inland waters). Top-down estimates are shown on the left as light-colored boxes and bottom-up estimates on the right as dark-colored boxes. Sectoral emission estimates based on less than 5 data points are shown as open boxes and those with 5 or greater data points are shown as filled boxes. The box represents the 25th to 75th percentile range, "x" represents the outliers, and the whiskers show the minimum and maximum values (outliers excluded)

BU = 75% (TD = 81%), totaling BU = 52 [49–59] (TD = 42 [37–56]) Tg $CH_4$ $yr^{-1}$, are driven by a roughly 50:50 split of *Fossil* and *Ag&Waste* emissions. In comparison, Brazil and Southeast Asia (along with Southwest South America, Central America, and Oceania), show strong *Ag&Waste* emissions, 31% (33%) and 32% (38%), respectively, accompanied by high *Wetl* emissions, 45% (58%) and 39% (38%), respectively. The majority of South Asian $CH_4$ emissions, 68% (64%), come from *Ag&Waste*. Finally, the USA emissions are split relatively evenly between natural emissions (*Wetl* + NonWetl), *Fossil* and *Ag&Waste* with 45% (30%), 25% (27%), and 29% (42%), respectively.

### *Fossil fuel*

*Fossil* emissions are defined here as the sum of coal, oil, gas, industrial and transport emissions, including fugitive emissions from exploration, production, and distribution. This sector can in turn be broken down in to four subsectors: *Coal*, *Oil&Gas*, *Industry*, and *Transport*. Emissions hotspots include China, Russia, the Middle East, and the USA who together produced 75 [67–82] (53 [46–77]) Tg $CH_4$ $yr^{-1}$ over the 2008–2017 period. This equates to 60% (49%) of total global *Fossil* $CH_4$ emissions, which were 124 [110–143] (107 [88–139]) Tg $CH_4$ $yr^{-1}$ (Figure S3b). Although TD emissions estimates are unable to inform a deep sectoral attribution of these emissions, BU emissions inventories can. These inventories suggest different sub-sectoral mixes between these regions with Chinese *Fossil* emissions dominated (> 80%) by *Coal*, the United States showing a shift from *Coal* to *Oil&Gas* emissions (from 30% to 10% *Coal* and from 60 to 80% *Oil&Gas* over the 2000 to 2017 period), and Russian and Middle Eastern emissions predominantly (>80%) *Oil&Gas* related (Höglund-Isaksson et al., 2020; Janssens-Maenhout et al., 2019; USEPA, 2012). A detailed subsectoral breakdown of the *Fossil* sector for all 19 regions and each of the four BU inventories is given in Figure S4.

### *Agriculture and waste*

Together South Asia and China account for 32% (33%) of all global *Ag&Waste* emissions producing 65 [61–69] (71 [64–77]) Tg $CH_4$ $yr^{-1}$ between 2008 and 2017 (Figure S3a). A second group of regions, South East Asia, Europe, USA, and Brazil, produce >15 Tg $CH_4$ $yr^{-1}$ each over the same period and in combination account for a further 34% (37%) of global emissions. For the following discussion, we decompose the *Ag&Waste* sector into three subsectors: *Livestock*, *Waste*, and *Rice*.

Although the exact distribution of Chinese sub-sectoral *Ag&Waste* emissions differs between BU inventories (Figure S5) most suggest a relatively even split during 2008–2017 between the *Livestock* (31%–44%), *Rice* (22%–31%), and *Waste* (31%–38%) sectors (Höglund-Isaksson et al., 2020; Janssens-Maenhout et al., 2019; USEPA, 2012). This distribution is significantly different to the South Asian sectoral distribution where *Livestock* alone accounts for 48 to 63% of these types of emissions with the remaining emissions split between *Waste* (18%–23%) and *Rice* (19%–32%). The predominance of *Livestock* emissions is again apparent in the Brazil, Europe, and USA with an average of 81%, 60%, and 56%, respectively, of all 2008–2017 *Ag&Waste* emissions coming from *Livestock*.

*Biomass burning and biofuels*

The *BB&F* emissions (composed of *Biomass Burning* and *Biofuel* emissions) are generally higher in the African regions with 33% (31%) of total global 2008–2017 *BB&F* emissions, 8 [8–9] (9 [8–10]) Tg $CH_4$ $yr^{-1}$, coming from the African continent due to extensive savanna burning. Other regional hotspots of *Biomass Burning* include Southeast Asia 14% (18%), China 13% (13%), South Asia 11% (9%), Brazil 6% (7%), and Russia 5% (6%).

Globally, BU emission inventories together with satellite biomass burning products indicate a roughly 50:50 split between *Biofuels* and *Biomass Burning*; however, this is not common across individual regions (Höglund-Isaksson et al., 2020; Janssens-Maenhout et al., 2019; Randerson et al., 2012; USEPA, 2012). The regions with the largest populations in this study, China and South Asia, show predominantly (87%–95%) *Biofuel* emissions driven by the use of biofuels for cooking and household heating in rural areas. In comparison, Brazil and Southern Africa, regions with significant deforestation and drought- and human-induced fire activity (Andela & van der Werf, 2014; Aragão et al., 2018), show mostly (78 to 91%) *Biomass Burning* emissions. Although the proportion of *Biomass Burning* to *Biofuel* emissions are generally relatively constant over time within a given region the Southeast Asian region shows a unique pattern. This region has fairly constant *Biofuel* emissions across the 2000–2017 time period of about 1 Tg $CH_4$ $yr^{-1}$; however, mean *Biomass Burning* emissions show significant IAV, fluctuating between 0.8 and 5 Tg $CH_4$ $yr^{-1}$ (Figure S1).

Ratios of *Biofuel* to *Fossil* emissions vary between regions and between BU inventories (due to differing biofuel sectorial definitions, see Supplementary S5). However, the relative regional rankings are fairly consistent between BU inventories with South Asia, Equatorial Africa, and Southern Africa showing the highest *Biofuel*:*Fossil* fuel ratios, averaging 0.5, 0.3, and 0.2, respectively (Figure S6).

*Wetlands*

*Wetl* emissions show a distinctive spatial distribution with the three largest contributing regions, Brazil, 15% (19%), Southeast Asia, 15% (12%), and Equatorial Africa, 14% (11%), of total *Wetl* emissions (147 [101–186] (168 [145–204]) Tg $CH_4$ $yr^{-1}$) all located on the equator. *Wetl* emissions are also a significant proportion of total emissions in these regions with 45% (58%), 39% (38%), and 41% (46%) of the total regional emissions coming from *Wetl* for Brazil, Southeast Asia, and Equatorial Africa, respectively. Other key contributing regions emitting >10 Tg $CH_4$ $yr^{-1}$ each, include Southwest South America, Russia, and Canada. On a continental basis South America emits 33% (34%) of all global *Wetl* emissions averaging 48 [36–60] (57 [52–65]) Tg $CH_4$ $yr^{-1}$ during the 2008–2017 period.

### 3.1.4 | Total emission rates and temporal trends

The overall temporal trends in TD and BU $CH_4$ emission means are very similar within each region, with all but one region (Canada) showing agreement in the direction (positive or negative) of trends (Figure 5 and Figure S7). Like global $CH_4$ emissions, which have been steadily increasing over the 2000–2017 period, most regions show an increase in total $CH_4$ emissions over time. Only Europe and the combined Korea & Japan region exhibit a decrease in total $CH_4$ emissions between 2000 and 2017. While absolute emission rates often differ between TD and BU estimates (Figure 5) no region, including Canada, shows a statistically significant difference between the TD and BU emission trend (slope) over the 2000 to 2017 period (student t-test, $p = .05$, See Supplementary S4).

Global emissions have increased on average, BU = 4 (TD = 3) Tg $CH_4$ $yr^{-1}$ $yr^{-1}$ or BU = 0.7 (TD = 0.6) % $yr^{-1}$ relative to 2000. However, rates of change differ between regions (Figure 5 and Figure S7). For instance, China increased at more than double the global rate, 2.4 (1.5) % $yr^{-1}$ relative to 2000. In contrast, Europe and Korea and Japan declined by 0.7 (0.5) and 0.2 (1) % $yr^{-1}$ relative to 2000, respectively (Figure S6b).

Both TD and BU estimates link the reduction in European emissions to a 28% (15%) decline in *Fossil* emissions and a 17% (11%) decline in *Ag&Waste* emissions since 2000. BU inventories that separate *Coal* emissions from other *Fossil* emissions show that declines are driven by decreases in *Coal* emissions (>20% relative to 2000) (Höglund-Isaksson et al., 2020; Janssens-Maenhout et al., 2019; USEPA, 2012). The GAINS and USEPA inventories show a concurrent decrease in *Oil&Gas* emissions (Höglund-Isaksson et al., 2020; USEPA, 2012).

BU inventories indicated that changes in European *Ag&Waste* emissions were evenly split between reductions in *Livestock* emissions (1–2 Tg $CH_4$ $yr^{-1}$, 9–15% relative to 2000) and reductions in *Waste* emissions (2–3 Tg $CH_4$ $yr^{-1}$, 27–30% relative to 2000) (Hoesly et al., 2018; Höglund-Isaksson et al., 2020; Janssens-Maenhout et al., 2019; USEPA, 2012). Inventories that provide further sub-sectoral information show that the decrease in *Waste* emissions are solely driven by solid waste (landfill and incineration) processing (Janssens-Maenhout et al., 2019) and that the majority of the *Livestock* emissions reductions are due to decreases in enteric fermentation.

The sectoral drivers of decline in Korean and Japanese emissions are not consistent between the four BU inventories. All four inventories show small (0.1 to 0.3 Tg $CH_4$ $yr^{-1}$) decreases in *Rice&Livestock* and *Waste* emissions, relative to 2000 with the subsector breakdown of the EDGAR, GAINS and USEPA

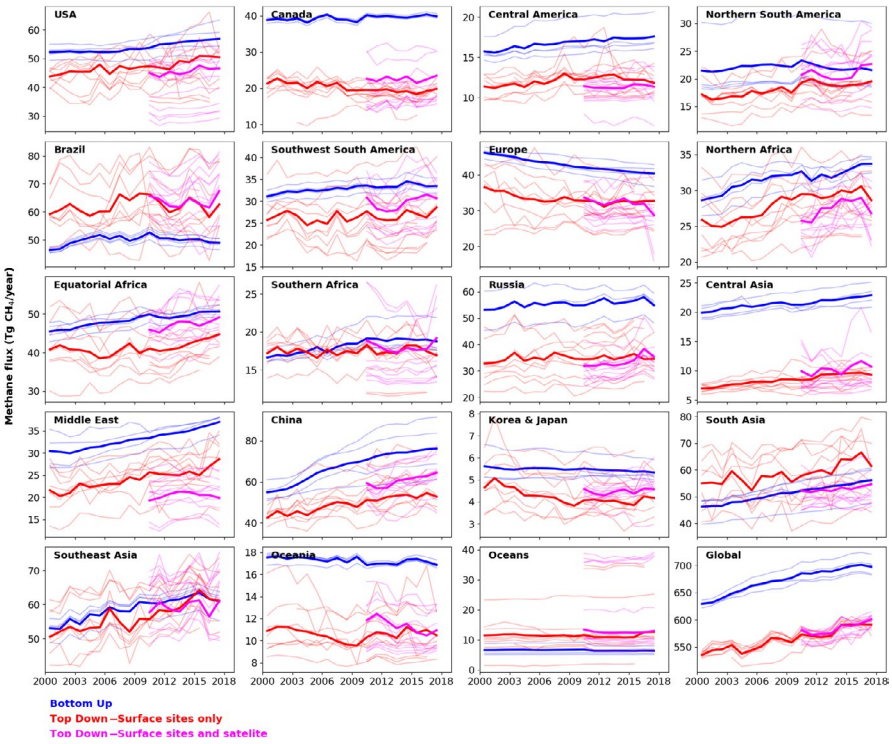


**FIGURE 5** Annual estimates of total $CH_4$ emissions in Tg $CH_4$ $yr^{-1}$ for each of the 18 land regions, the ocean region and the global total over 2000–2017. Bottom-up (blue) and top-down (red—surface sites only, magenta—surface sites and satellite data). Thick lines indicate the mean estimate, whereas thin lines represent individual estimates

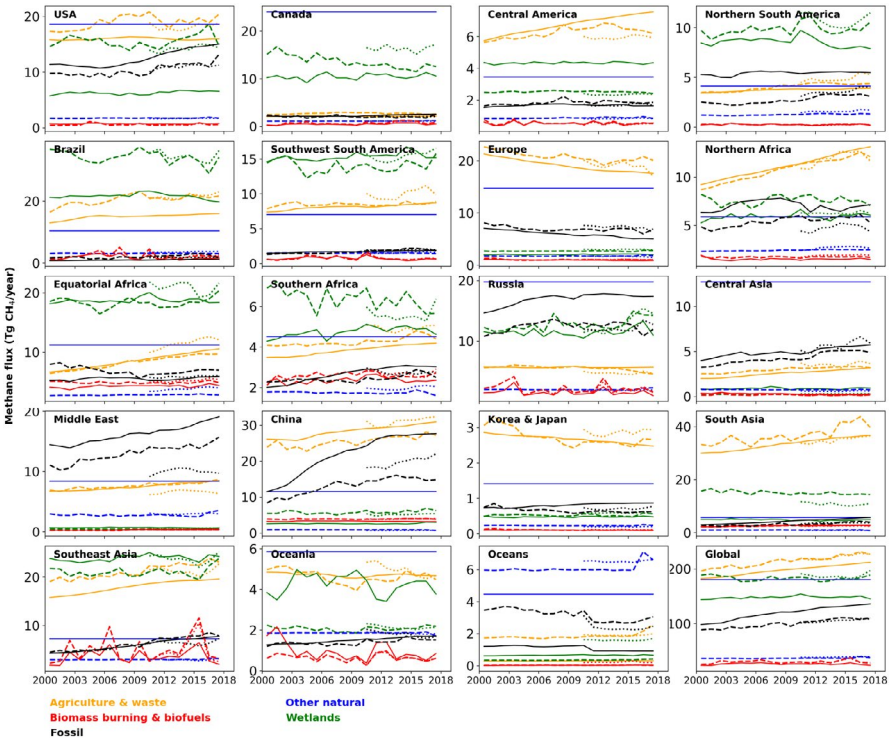


**FIGURE 6** Yearly mean regional and global agriculture and waste (orange), biomass burning and biofuel (red), fossil fuels (black), other natural (blue) and wetland (green) fluxes in Tg $CH_4$ $yr^{-1}$ over 2000 to 2017. The mean of the bottom-up estimates are shown as a solid line, the mean of the top-down (surface sites only) as a dashed line and the mean of the top-down estimates including GOSAT data as a dotted line

inventories attributing the decline in *Rice&Livestock* to the *Rice* sector. However, *Fossil* emission trends differ with the CEDS and USEPA inventories showing an increase of 0.2–0.4 Tg $CH_4$ $yr^{-1}$ and the more recent inventories, EDGAR and GAINS, a small decline (−0.04 to −0.06 Tg $CH_4$ $yr^{-1}$) (Figure S10). In contrast, all TD emissions estimates show a decline in both total *Fossil* and *Ag&Waste* emissions (Figure 6).

Both China and the Middle East, regions with emissions rates significantly higher than the global mean, show significant increases in *Fossil* and *Ag&Waste* emissions over the 2000–2017 period. *Fossil* emissions from China increased by 141% (78%) (See also Section 3.2.3) and *Ag&Waste* by 18% (14%), between 2000 and 2017, whereas Middle Eastern *Fossil* and *Ag&Waste* emissions have climbed by 32% (42%) and 26% (26%), respectively, over the

same period. The EDGAR BU inventory alone suggests that the Middle East increase in *Fossil* emissions is dominated by increases in natural gas related emissions (Janssens-Maenhout et al., 2019), while all inventories agree on increases in *Livestock* and *Waste* emissions (Hoesly et al., 2018; Höglund-Isaksson et al., 2020; Janssens-Maenhout et al., 2019; USEPA, 2012).

Only Southeast Asia and Russia show similar patterns in TD and BU mean IAV. A sectoral decomposition of these regions (Figure 6) shows that this IAV is driven by a combination of *WetI* and *BB&F*.

Although the absolute magnitude of the TD and BU total emissions estimates differ significantly for most regions, there are some regions, the United States, Southeast Asia, and the three African regions, which appear to agree well (average absolute difference 2000 to 2017 < 15%, SURF data only). On average, absolute differences between regional TD and BU estimates decrease by 3% with the addition of the GOSAT data. Agreement tends to improve in equatorial regions with a paucity of long-term ground-based observations (Figure 1). Specifically, Northern South America, Southwest South America, Equatorial Africa, and South Asia show a reduction in TD and BU total emission difference of >7% when using both GOSAT and SURF data (2010 to 2017) (Figure S8).

Some regions, including the United States, Central Asia, and Northern Africa, show an acceleration in emissions post 2010 (Figure 5). Both BU and TD methods link the USA post-2010 increase to the *Fossil* sector (Figure 6) with the GAINS and EDGAR BU estimates indicating a >100% increase in *Oil&Gas* emissions. Other regions, for example Brazil, show a small decline in emissions between 2009 and 2017 with sectoral estimates linking this to a 14% (9%) decline in *WetI* emissions.

## 3.2 | Top-down and bottom-up differences

### 3.2.1 | Total $CH_4$ emissions

As identified in Saunois et al. (2020) and demonstrated again here, there is a significant difference in the global TD and BU total emissions estimates, most likely driven by double counting of fluxes from wetlands and inland waters, and extrapolation issues (e.g., Thornton et al., 2016). Here we find the 2008–2017 median BU estimate to be 136 Tg $CH_4$ $yr^{-1}$ higher than the median TD estimate. This offset (along with the total and sectoral TD and BU emission estimates) differs from that of Saunois et al. (2020) as here we exclude the GOSAT estimates from the decadal means, use a new inland waters estimate and use one less BU agricultural estimate (See Section 2). However, although the 2008–2017 global mean BU total of this paper is 48 Tg $CH_4$ $yr^{-1}$ lower than the Saunois et al. (2020) mean it is within the (wide) range of their global BU emissions estimates, 594 to 881 Tg $CH_4$ $yr^{-1}$. Our lower estimate is predominantly due to a lower inland waters estimate, 129 cf. 159 Tg $CH_4$ $yr^{-1}$, and a lower oceanic emissions estimate 3 cf. 13 Tg $CH_4$ $yr^{-1}$.

For 18 of the 19 regions TD total $CH_4$ posterior emission estimates are closer to their prior than the BU estimate (Figure 2). However, this trend is not consistent across the subsectors (e.g., Fossil, Figure S3b). For 16 of the 19 regions examined median regional BU estimates of total $CH_4$ flux are higher than posterior TD estimates (Figure 2). However, only four regions (Canada, Central Asia, Russia, and Oceania, Figure 2) do not agree within the 25th-75th percentile range, with all these regions showing total BU ≫TD. As with global estimates regional BU–TD discrepancies are driven by BU *NonWetI* emissions estimates (Figure S3a–d cf. S3e), primarily elevated *Inland Water* emissions (Figure S9).

Although TD sectoral partitioning can be problematic (Section 2.2), it is interesting that for the two land regions with higher TD than BU estimates, Brazil and South Asia, this difference is caused primarily by *WetI* emissions. Here the Brazil and South Asia TD *WetI* estimates, 33 [31–35] and 13 [11–15] Tg $CH_4$ $yr^{-1}$, respectively, are >45% higher than the BU estimates, 23 [15–28] and 4 [3–5] Tg $CH_4$ $yr^{-1}$ (Figures 4 and 6). Even though this is a large discrepancy between median estimates, there are some BU wetland models that do find higher *WetI* emissions. For example, the LPX-Bern model has a Brazilian mean 2008–2017 *WetI* emission estimate of 31 Tg $CH_4$ $yr^{-1}$ and the DLEM model a South Asian mean 2008–2017 *WetI* emission estimate of 16 Tg $CH_4$ $yr^{-1}$ (see Table 2 Saunois et al. (2020) for further information on individual wetland models). In addition, the mean of BU wetland models run using a prognostic extent mode (where wetland extent is determined by the model) is significantly closer to those of the TD estimates for these two regions, 40 and 11 Tg $CH_4$ $yr^{-1}$ for Brazil and South Asia, respectively. While the higher TD *WetI* estimates may not be correct there are known issues with wetland mapping, particularly in flooded forest regions where closed canopies make remote sensing of water-saturated soils challenging (Prigent et al., 2020). As such, the TD-BU *WetI* discrepancy along with the difference in prognostic and diagnostic BU wetland models suggests that there may be room for improvement in the diagnostic wetland map in the Brazilian and South Asian regions. It is also interesting to note that the addition of the GOSAT data to the TD inversion estimate decreases the TD *WetI* estimate in the South Asia region by approximately 5 Tg $CH_4$ $yr^{-1}$. This result suggests that where surface site numbers are limited (Figure 1) the TD-BU discrepancy may be partially driven by data coverage, emphasizing the importance of satellite data.

### 3.2.2 | Temporal trends in total $CH_4$ emissions

Canada is the only region to show a statistically different trend in TD and BU emissions, with TD estimates showing a gradual decrease in $CH_4$ emissions and BU estimates showing an increase (Figures 5 and 6). The sectoral breakdown of the BU and TD emissions estimates shows this difference to be driven by *WetI* emissions with a downward trend in *WetI* emissions, ~0.3 Tg $CH_4$ $yr^{-2}$, present in all but one of the TD SURF emissions estimates. This contrasts with BU process model estimates which, while varying in absolute magnitude, all show a small upward trend in *WetI* emissions.

### 3.2.3 | Sectoral $CH_4$ emissions

As discussed earlier (Section 3.2.1), high BU *Inland Waters* estimates drive discrepancies in TD and BU total emissions estimates. These also lead to higher BU estimates of natural emissions (Figure 3a) and in turn (for all regions other than South Asia), higher TD estimates of anthropogenic proportion (Figure 3c). The discrepancy in the Central Asia region is particularly large with a median TD anthropogenic proportion of 89% and a BU estimate of 37%. This difference is driven by the far higher (~15 times) BU estimate of natural emissions, 86% of which is *Inland Waters* (Figure S9). Unlike land region estimates, in the ocean region a higher TD estimate of anthropogenic proportion, is driven by a higher (~3.5 times) TD estimate of anthropogenic *Fossil* emissions.

Figure 6 shows annual mean values for the TD and BU sectoral emissions estimates for the 2000 to 2017 period. This figure shows clear differences between the temporal trends in TD and BU estimates of *WetI*, *NonWetI* (both discussed previously in Section 3.2.1) and *Fossil* emissions for many regions. While there can be significant methodologically driven uncertainties with TD sectoral estimates (Section 2), when optimising for total $CH_4$ fluxes seven of the nine TD estimates (Table S1) used here are independently optimized for at least anthropogenic (if not *Fossil* specific) emissions. As such, the TD *Fossil* estimates while treated with caution are reported here and used to inform the discussion.

For most regions, the TD and BU *Fossil* estimates are similar over the 2000–2017 period; however, there are notable differences, particularly for China, the Middle East, Russia, and Northern South America where TD and BU estimates differ by up to 10 Tg $CH_4$ $yr^{-1}$. During the year 2000 the Chinese CEDS *Fossil* estimate (upper blue line, Figure S10) is similar to the other three BU inventories but then rapidly accelerates and by 2017 is almost double that of the other three BU inventories. As noted earlier, the *Fossil* component of the CEDS inventory is based on an earlier EDGAR v4.2 inventory which is known to overestimate *Coal* emissions in China (See Section 2.1.1). However, limiting the analysis to the remaining three BU inventories only reduces the annual mean TD and BU difference by 20%. In fact, the mean BU estimate (CEDS excluded) is consistently higher than all but two of the individual TD estimates with only one of the BU estimates, USEPA, within the range of the majority of the TD estimates. A closer examination of the sub-sectoral breakdown of the BU inventories suggests that the EDGAR and GAINS *Fossil* estimates are higher than the other inventories due to a combination of higher *Oil&Gas* emissions (10 times the USEPA inventory, Figure S4) and *Coal* emissions (up to 50% higher than the USEPA inventory, Figure S4).

There are large discrepancies between the TD and individual BU inventory estimates of Northern South American *Fossil* emissions (Figure S10). The CEDS estimate is consistently (> 4 times) higher than the other three BU inventories and the TD estimates (Figure S4 and S10). Interestingly, a closer examination of the gridded CEDS data shows the majority of these emissions occurring from a single point source in Venezuela. This assessment agrees with other inversion studies (Maasakkers et al., 2019; Y. Zhang et al., 2020), which suggest an under-estimate in Venezuelan *Oil&Gas* emissions in the EDGAR and UNFCCC estimates. However, Maasakkers et al. (2019) only revised these estimates to ~5 Tg $CH_4$ $yr^{-1}$, that is, far less than the ~12 Tg $CH_4$ $yr^{-1}$ allocated by the CEDS emission inventory.

## 4 | DISCUSSION

### 4.1 | Emissions and policy relevance

Four key regions (China, South Asia, Southeast Asia, and the United States) together account for >40% of global anthropogenic $CH_4$ emissions (Figure 3 and Figure S2a). Most of these emissions come from a combination of the *Fossil* (in particular *Coal* and *Oil&Gas*) and *Ag&Waste* (in particular *Livestock)* sectors (Section 3.1.3). The predominance of *Fossil* and *Ag&Waste* emissions in these regions of high total $CH_4$ emissions highlights the importance of these sectors as opportunities for significant emissions mitigation.

In general, anthropogenic emissions can be divided into three groups roughly correlating with the size of their regional populations (Figure 3 and Figure S2). The group 1 regions (China and South Asia), those with the largest anthropogenic emissions (combined >25% of global anthropogenic emissions) are also the regions with the largest populations (>40% of the global population (United Nations, 2019)), whereas the second group of regions account for >55% of anthropogenic emissions and the third group <20%. This breakdown suggests that relatively large mitigation opportunities exist in group 1 and 2 nations, while smaller but substantial opportunities exist in other regions.

China has the largest anthropogenic $CH_4$ emissions of any region (> 13% of the total) and one of the fastest growing trends with a BU = 51% (TD = 27%) increase between 2000 and 2017. This growth is driven predominantly by increases in *Coal* and *Ag&Waste* emissions, with BU inventories suggesting that the increase in Chinese *Coal* emissions alone accounts for >15% of the global total emissions increase. Increases in Chinese coal mining activities have been linked to rapid economic growth, which relies predominantly on coal-based energy sources (Jackson et al., 2018; Miller et al., 2019; Peters et al., 2017). However, recent Chinese inventory studies suggest a decline in coal mining emissions since 2012 (Gao et al., 2020; Sheng et al., 2019). Similarly, increases in Chinese *Waste* emissions have been driven by economic growth and urbanization. This sector, however, has great mitigation potential as previous work reports that changes in landfill procedures could lead to a 30%–50% reduction in landfill emissions (Cai et al., 2018). The increases in agricultural $CH_4$ emissions are being driven by diet changes associated with the rising standard of living and the promotion of the agricultural economy (Tian et al., 2014; Zhang & Chen, 2010). Tian et al. (2014) also emphasize that given China's economic dependence on agriculture, decreases in agricultural emissions will only come from changes in production methods not a reduction in agricultural capacity.

In contrast, anthropogenic emissions from Europe and Korea & Japan have decreased by 20% (13%) and 7% (14%), respectively. Specifically, decreases in European *Livestock* emissions (mainly enteric fermentation) have been linked to decreases in livestock numbers driven by reforms to the EU common agricultural policy (CAP) (EUROSTAT, 2017; Vergé et al., 2007). However, livestock numbers have remained unchanged since 2008 (FAO, 2019a) and future reductions may instead need to come from changes in farm management, feed composition, and additives and selective breeding (EIP-AGRI, 2017; Pellerin et al., 2014; Roque et al., 2021). Reductions in European solid waste emissions have been driven by the EU Landfill Directive 1999/31/EC which aimed to reduce the amount of biodegradable waste entering landfills sites (EUROSTAT, 2014). Although the economic and policy drivers of European $CO_2$ emissions have been examined in detail elsewhere (e.g., Le Quéré et al. (2019)), similar studies of $CH_4$ appear lacking in the literature. Reports describing total Japanese greenhouse gas emissions (as opposed to solely $CH_4$ emissions) link the decline in these emissions to the adoption of renewable energy, a resumption of nuclear energy and a reduction in energy consumption due to improved energy conservation and reduced manufacturing production (Ministry of the Environment, 2021). This agrees well with the reductions in TD *Fossil* emissions and those of the *Coal* sector evident in the GAINS and EDGAR BU estimates. Similarly, reductions in Japanese *Waste* and *Rice* emissions (evident in EDGAR, GAINS and USEPA inventory estimates) align with Japanese governmental policies which propose decreasing methane emissions through the reduction of landfill organic waste disposal and altering rice farming practices (Ministry of the Environment, 2014). However, decreases in these emission estimates were evident prior to the 2014 policies making the contribution of environmental policy unclear.

Several TD studies have found that USA anthropogenic (in particular *Oil&Gas* and *Livestock*) emissions are underestimated in BU inventories (e.g., Maasakkers et al., 2021; Williams et al., 2021; Y. Zhang et al., 2020). Considering that the United States is the third largest contributor to global anthropogenic emissions and that BU, rather than TD, estimates are used to track and assess policy outcomes, resolving this discrepancy would be valuable. However, while the median BU USA anthropogenic emissions estimate (28 Tg $CH_4$ $yr^{-1}$ for 2008–2017) is lower than the TD estimate (31 Tg $CH_4$ $yr^{-1}$), they do agree within the 25th-75th percentile range (Figure 3) and as such our data suggest that the methods may well be consistent.

## 4.2 | Methodological and science implications

In this paper, we explored a range of TD and BU emission estimates with the aim of providing policy-relevant information with sector-specific emissions and trend data that are necessary for developing effective regional $CH_4$ mitigation strategies and protocols. Because of methodological limitations (Sections 2.2 and 3.2.3), comparisons between TD and BU emission estimates should be treated with care. However, our comparisons of Brazilian and South Asian TD and BU *WetI* estimates (Section 3.2.1) and TD and BU *Fossil* estimates (Section 3.2.3) demonstrate their power to identify methodological issues in current reporting approaches and areas requiring further study, while, clearly useful in their current form, TD and BU estimates could be improved.

Regional BU inventory estimates could be enhanced with the implementation of time varying regional and technologically specific emissions factors and checks on the reported activity data. There are also significant differences in the spatial distribution of sectoral emissions between inventories suggesting that further work is required to accurately map emissions regionally. Encouragingly, efforts to implement these suggestions and to use TD estimates to inform and improve European BU inventory estimates are already underway as part of the VERIFY project (https://verify.lsce.ipsl.fr/index.php). However, it is important that such efforts are implemented world-wide, particularly in other regions with large anthropogenic emissions.

The low accuracy of natural flux estimates limits our ability to separate anthropogenic and natural flux estimates. Required improvements are the development of gridded inland water estimates, supported by a long-term global inland water monitoring network, the development of process-based models, use of observed site-level $CH_4$ emissions for model benchmarking (e.g., FLUXNET-$CH_4$; Delwiche et al. (2021)), and the avoidance of double counting with the use of comprehensive inland water models encompassing all water body types (e.g., lakes, ponds, and rivers) and using spatial masks consistent with those used by wetland models.

Many TD methods rely on the use of fixed OH climatology (i.e., no IAV) which may artificially bias TD emissions estimates. In our study, emissions calculated with independent OH field optimization (allowing for IAV) show similar or only slightly larger $CH_4$ emissions than those without OH IAV. Similarly, Zhao et al. (2019) examined a range of OH scenarios and suggested that IAV OH offsets 7–20% of the increase in global $CH_4$ emissions between 2000 and 2010. This increase roughly equates to a global emissions reduction of 3–11 Tg $CH_4$ $yr^{-1}$. Although small compared with the global 136 Tg $CH_4$ $yr^{-1}$ TD-BU discrepancy, any improvement in accuracy is important. Similarly, the spatial distribution of the TD chemical sink prior can influence the regional distribution of TD-derived $CH_4$ sources. However, this effect is likely to be small with Zhao et al. (2019) finding that large (~50%) variability in the OH spatial distribution only equated to a 1.5% variability in regional $CH_4$ mixing ratios. While only a proxy for variability in the true OH $CH_4$ sink this in an order of magnitude smaller than the mean range of TD emissions estimates and easily contained within the current uncertainty range.

Other key developments in TD approaches include improvements in atmospheric transport models (especially vertical transport, stratospheric transport and the simulation of boundary layer dynamics), methodological improvements in TD sector-specific flux estimation using isotopic tracers and co-emitted compounds (e.g., ethane) as additional constraints and the use of the latest satellite data (e.g., TROPOMI http://www.tropomi.eu).

## 5 | CONCLUSIONS

Five regions—China, Southeast Asia, USA, South Asia, and Brazil—account for >40% of all $CH_4$ emissions during the decade of 2008–2017. Emissions from most of these regions, like global emissions, are equally contributed by anthropogenic and natural sources, except China and South Asia where emissions are predominantly (> 75%) anthropogenic. *Livestock* (46%) and *Rice* (20%) account for the bulk of anthropogenic emissions from South Asia, whereas *Fossil* accounts for 40% of China's anthropogenic emissions with most of the remaining emissions equally distributed between *Livestock*, *Rice* and *Waste*.

Annual global $CH_4$ emissions increased by ~10% (50–70 Tg $CH_4$) between 2000 and 2017 (Jackson et al., 2020). Regionally China, the Middle East, South Asia, and Southeast Asia are the largest contributors to this rise, together accounting for 62–67% (33–46 Tg $CH_4$) of the global increase. Increases in China and the Middle East are driven by *Fossil* emissions, with the increase in *coal* emissions from China alone accounting for ~15% of the global emissions increase. Increases in South Asia are related predominantly to *Livestock* and *Waste*, whereas those in Southeast Asia are more equally divided between *Coal*, *Rice*, *Livestock* and *Waste* emissions.

In contrast, emissions from Europe and Korea and Japan decreased by ~10%. European emissions reductions were linked to decreases in *Waste* (mainly solid waste disposal), *Livestock* and *Coal*, which on average accounted for 43%, 26%, and 22% of the decline, respectively. Japanese emissions decline at a similar rate to European emissions, driven by reductions in *Waste* and *Rice* emissions, however absolute emissions are an order of magnitude smaller.

The *Coal*, *Waste*, and *Livestock* subsectors are common drivers of rapid increases and decreases in regional $CH_4$ emissions. As such, these sectors present the best opportunities for $CH_4$ emissions mitigation and the largest risks (drivers) of on-going emission increases.

Regions with significant natural emissions (e.g., Brazil with 22–34 Tg $CH_4$ $yr^{-1}$ from *Wetl)* are also key, with the influence of climate change on these sources an area of concern. Some studies (e.g., Zhang et al., 2018) suggest that changes in temperature and precipitation patterns may have already led to increases in $CH_4$ *Wetl* emissions growth rates. However, as these flux types have no or limited mitigation potential the focus when implementing emission reduction schemes should be on regions with a large proportion of anthropogenic emissions.

Considering the large contribution of Global $CH_4$ emissions to the Earth's radiative budget, the predominance of increasing (rather than decreasing) $CH_4$ emissions is a large concern. However, the emissions decline observed in Europe and Korea and Japan provides evidence that a decrease in emissions in response to government policies and/or economic forces is possible.

### ACKNOWLEDGMENTS

This paper is the result of a collaborative international effort under the umbrella of the Global Carbon Project, a Global Research Project of Future Earth and a research partner of the World Climate Research Programme. We acknowledge primary support for the methane budget from the Gordon and Betty Moore Foundation through Grant GBMF5439 "Advancing Understanding of the Global Methane Cycle" to Stanford University (P.I. Rob Jackson; co-P.I.s Philippe Bousquet, Marielle Saunois, Josep Canadell, Gustaf Hugelius, and Ben Poulter). Josep Canadell acknowledges the support of the Australian National Environmental Science Program – Earth Systems and Climate Change. Prabir K Patra and Neveen Chandra acknowledge support from Environment Research and Technology Development Funds of the Environmental Restoration and Conservation Agency of Japan (JPMEERF20182002, JPMEERF20172001). Jurek Müller thanks for support by the Swiss National Science Foundation (#200020_172476). Peter Bergamaschi acknowledges the support of ECMWF providing computing resources under the special project "Improve European and global $CH_4$ and $N_2O$ flux inversions (2018-2020)". Pierre Regnier acknowledges the support from the VERIFY project under European Union's Horizon 2020 research and innovation program grant agreement no. 776810. The TM5-CAMS inversions are available from https://atmosphere.copernicus.eu; Arjo Segers acknowledges the support from the Copernicus Atmosphere Monitoring Service, implemented by the European Centre for Medium-Range Weather Forecasts on behalf of the European Commission (grant no. CAMS73). William Riley acknowledges support by the US Department of Energy, Office of Science, Biological and Environmental Research, Regional and Global Climate Modeling Program through the RUBISCO Scientific Focus Area under contract DE-AC02-05CH11231 to Lawrence Berkeley National Laboratory. The authors gratefully acknowledge those responsible for the global network of atmospheric observations used in this study including Donald R Blake and Isobel Simpson, University of California Irvine, USA; Gordon Brailsford, NIWA, Cyril Crevosier, LMD, France; New Zealand; Paul Krummel and Ray Langenfelds, CSIRO, Australia; Toshinobu Machida, Yasunori Tohjima and Yukio Yoshida, NIES, Japan; Ronald Prinn, MIT, USA; Simon O'Doherty, University of Bristol, UK; Michel Ramonet, LSCE-IPSL, France; Atsushi Takizawa, JMA, Japan; Ray Weiss, Scripps Institute of Oceanography, USA and Doug Worthy, Environment Canada, Canada. We would also like to thank Lena Höglund-Isaksson, IIASA, Austria, Greet Janssens-Maenhout EC-JRC, Italy and Steven Smith, PNNL-JGCR, USA for their assistance with the anthropogenic inventory data. The authors also acknowledge the significant contribution of Goulven G. Laruelle, Department Geoscience, Environment & Society, Université Libre de Bruxelles, Brussels, Belgium who, with P. Regnier, developed the regionally distributed estuarine flux data set.

### CONFLICT OF INTEREST

The authors declare that there are no competing financial interests.

### DATA AVAILABILITY STATEMENT

A number of data sets were used to support the findings of this study. These data sets are either openly available in repositories as listed in the text and references, available on request from the original developers (see text and references there in) or are available from the corresponding author upon reasonable request.

## ORCID

*Ann R. Stavert* https://orcid.org/0000-0002-4857-2134
*Marielle Saunois* https://orcid.org/0000-0003-3983-2931
*Josep G. Canadell* https://orcid.org/0000-0002-8788-3218
*Benjamin Poulter* https://orcid.org/0000-0002-9493-8600
*Robert B. Jackson* http://orcid.org/0000-0001-8846-7147
*Ronny Lauerwald* https://orcid.org/0000-0001-5554-0897
*Prabir K. Patra* https://orcid.org/0000-0001-5700-9389
*Naveen Chandra* https://orcid.org/0000-0002-5357-7757
*Shamil Maksyutov* https://orcid.org/0000-0002-1200-9577
*Joe R. Melton* https://orcid.org/0000-0002-9414-064X
*Arjo Segers* https://orcid.org/0000-0002-1319-0195
*Hanqin Tian* https://orcid.org/0000-0002-1806-4091
*Yi Yin* https://orcid.org/0000-0003-4750-4997
*Qianlai Zhuang* https://orcid.org/0000-0002-4536-9851


## REFERENCES


Andela, N., & van der Werf, G. R. (2014). Recent trends in African fires driven by cropland expansion and El Niño to La Niña transition. *Nature Climate Change*, *4*(9), 791–795. https://doi.org/10.1038/nclimate2313

Anderson, D. C., Duncan, B. N., Fiore, A. M., Baublitz, C. B., Follette-Cook, M. B., Nicely, J. M., & Wolfe, G. M. (2021). Spatial and temporal variability in the hydroxyl (OH) radical: Understanding the role of large-scale climate features and their influence on OH through its dynamical and photochemical drivers. *Atmospheric Chemistry and Physics*, *21*(8), 6481–6508. https://doi.org/10.5194/acp-21-6481-2021

Aragão, L. E. O. C., Anderson, L. O., Fonseca, M. G., Rosan, T. M., Vedovato, L. B., Wagner, F. H., Silva, C. V. J., Silva Junior, C. H. L., Arai, E., Aguiar, A. P., Barlow, J., Berenguer, E., Deeter, M. N., Domingues, L. G., Gatti, L., Gloor, M., Malhi, Y., Marengo, J. A., Miller, J. B., … Saatchi, S. (2018). 21st Century drought-related fires counteract the decline of Amazon deforestation carbon emissions. *Nature Communications*, *9*(1), 536. https://doi.org/10.1038/s41467-017-02771-y

Balcombe, P., Speirs, J. F., Brandon, N. P., & Hawkes, A. D. (2018). Methane emissions: Choosing the right climate metric and time horizon. *Environmental Science: Processes and Impacts*, *20*(10), 1323–1339. https://doi.org/10.1039/C8EM00414E

Bergamaschi, P., Houweling, S., Segers, A., Krol, M., Frankenberg, C., Scheepmaker, R. A., & Gerbig, C. (2013). Atmospheric $CH_4$ in the first decade of the 21st century: Inverse modeling analysis using SCIAMACHY satellite retrievals and NOAA surface measurements. *Journal of Geophysical Research: Atmospheres*, *118*(13), 7350–7369. https://doi.org/10.1002/jgrd.50480

Bergamaschi, P., Karstens, U., Manning, A. J., Saunois, M., Tsuruta, A., Berchet, A., & Dlugokencky, E. (2018). Inverse modelling of European $CH_4$ emissions during 2006–2012 using different inverse models and reassessed atmospheric observations. *Atmospheric Chemistry and Physics*, *18*(2), 901–920. https://doi.org/10.5194/acp-18-901-2018

Cai, B., Lou, Z., Wang, J., Geng, Y., Sarkis, J., Liu, J., & Gao, Q. (2018). $CH_4$ mitigation potentials from China landfills and related environmental co-benefits. *Science Advances*, *4*(7), eaar8400. https://doi.org/10.1126/sciadv.aar8400

Chandra, N., Patra, P. K., Bisht, J. S. H., Ito, A., Umezawa, T., Saigusa, N., Morimoto, S., Aoki, S., Janssens-maenhout, G., Fujita, R., Takigawa, M., Watanabe, S., Saitoh, N., & Canadell, J. G. (2021). Emissions from the oil and gas sectors, coal mining and ruminant farming drive methane growth over the past three decades. *Journal of the Meteorological Society of Japan. Ser. II*, *99*(2), 309–337. https://doi.org/10.2151/jmsj.2021-015

Darmenov, A., & da Silva, A. (2015). *The quick fire emissions dataset (QFED): Documentation of versions 2.1, 2.2 and 2.4*. Retrieved from http://gmao.gsfc.nasa.gov/pubs/docs/Darmenov796.pdf

Delwiche, K. B., Knox, S. H., Malhotra, A., Fluet-Chouinard, E., McNicol, G., Feron, S., & Jackson, R. B. (2021). FLUXNET-CH4: A global, multi-ecosystem dataset and analysis of methane seasonality from freshwater wetlands. *Earth System Science Data*, *13*(7), 3607–3689. https://doi.org/10.5194/essd-13-3607-2021

EIP-AGRI. (2017). *EIP-AGRI focus group on reducing emissions from cattle farming*. Retrieved from Brussels: https://ec.europa.eu/eip/agriculture/sites/agri-eip/files/eip-agri_fg_livestock_emissions_final_report_2017_en.pdf

Etiope, G., Ciotoli, G., Schwietzke, S., & Schoell, M. (2019). Gridded maps of geological methane emissions and their isotopic signature. *Earth System Science Data*, *11*(1), 1–22. https://doi.org/10.5194/essd-11-1-2019

EUROSTAT. (2014). *Greenhouse gas emissions from waste disposal*. Retrieved from https://ec.europa.eu/eurostat/statistics-explained/index.php?title=Archive:Greenhouse_gas_emissions_from_waste_disposal

EUROSTAT. (2017). *Agri-environmental indicator - greenhouse gas emissions*. Retrieved from https://ec.europa.eu/eurostat/statistics-explained/pdfscache/16817.pdf

FAO. (2019a). FAOSTAT Agri-Environmental Indicators – Livestock Patterns. Retrieved November 11, 2019, from http://www.fao.org/faostat/en/#data/EK

FAO. (2019b). FAOSTAT. Food and Agriculture Organization of the United Nations. Statistical Division. Retrieved February 2019, from http://www.fao.org/faostat/en/#data

FAO. (2021). FAOSTAT. Food and Agriculture Organization of the United Nations. Statistical Division. Retrieved Feb 2021 http://www.fao.org/faostat/en/#data

Florez-Leiva, L., Damm, E., & Farías, L. (2013). Methane production induced by dimethylsulfide in surface water of an upwelling ecosystem. *Progress in Oceanography*, *112–113*, 38–48. https://doi.org/10.1016/j.pocean.2013.03.005

Gao, J., Guan, C., & Zhang, B. (2020). China's $CH_4$ emissions from coal mining: A review of current bottom-up inventories. *Science of the Total Environment*, *725*, 138295. https://doi.org/10.1016/j.scitotenv.2020.138295

GCP. (2021). Global methane budget. Retrieved from https://www.globalcarbonproject.org/methanebudget/

Hmiel, B., Petrenko, V. V., Dyonisius, M. N., Buizert, C., Smith, A. M., Place, P. F., Harth, C., Beaudette, R., Hua, Q., Yang, B., Vimont, I., Michel, S. E., Severinghaus, J. P., Etheridge, D., Bromley, T., Schmitt, J., Faïn, X., Weiss, R. F., & Dlugokencky, E. (2020). Preindustrial $^{14}CH_4$ indicates greater anthropogenic fossil CH4 emissions. *Nature*, *578*(7795), 409–412. https://doi.org/10.1038/s41586-020-1991-8

Hoesly, R. M., Smith, S. J., Feng, L., Klimont, Z., Janssens-Maenhout, G., Pitkanen, T., Seibert, J. J., Vu, L., Andres, R. J., Bolt, R. M., Bond, T. C., Dawidowski, L., Kholod, N., Kurokawa, J.-I., Li, M., Liu, L., Lu, Z., Moura, M. C. P., O'Rourke, P. R., & Zhang, Q. (2018). Historical (1750–2014) anthropogenic emissions of reactive gases and aerosols from the Community Emissions Data System (CEDS). *Geoscientific Model Development*, *11*(1), 369–408. https://doi.org/10.5194/gmd-11-369-2018

Höglund-Isaksson, L., Gómez-Sanabria, A., Klimont, Z., Rafaj, P., & Schöpp, W. (2020). Technical potentials and costs for reducing global anthropogenic methane emissions in the 2050 timeframe –results from the GAINS model. *Environmental Research Communications*, *2*(2), 025004. https://doi.org/10.1088/2515-7620/ab7457

IPCC. (2021). *Climate change 2021: The physical science basis. Contribution of Working Group I to the sixth assessment report of the intergovernmental panel on climate change*. Retrieved from https://www.ipcc.ch/report/ar6/wg1/

Jackson, R. B., Le Quéré, C., Andrew, R. M., Canadell, J. G., Korsbakken, J. I., Liu, Z., Peters, G. P., & Zheng, B. (2018). Global energy growth is outpacing decarbonization. *Environmental Research Letters*, *13*(12), 120401. https://doi.org/10.1088/1748-9326/aaf303

Jackson, R. B., Saunois, M., Bousquet, P., Canadell, J. G., Poulter, B., Stavert, A. R., Bergamaschi, P., Niwa, Y., Segers, A., & Tsuruta, A.

(2020). Increasing anthropogenic methane emissions arise equally from agricultural and fossil fuel sources. *Environmental Research Letters*, *15*(7), 071002. https://doi.org/10.1088/1748-9326/ab9ed2

Janssens-Maenhout, G., Crippa, M., Guizzardi, D., Muntean, M., Schaaf, E., Dentener, F., Bergamaschi, P., Pagliari, V., Olivier, J. G. J., Peters, J. A. H. W., van Aardenne, J. A., Monni, S., Doering, U., Petrescu, A. M. R., Solazzo, E., & Oreggioni, G. D. (2019). EDGAR v4.3.2 Global Atlas of the three major greenhouse gas emissions for the period 1970–2012. *Earth System Science Data*, *11*(3), 959–1002. https://doi.org/10.5194/essd-11-959-2019

Kaiser, J. W., Heil, A., Andreae, M. O., Benedetti, A., Chubarova, N., Jones, L., Morcrette, J.-J., Razinger, M., Schultz, M. G., Suttie, M., & van der Werf, G. R. (2012). Biomass burning emissions estimated with a global fire assimilation system based on observed fire radiative power. *Biogeosciences*, *9*(1), 527–554. https://doi.org/10.5194/bg-9-527-2012

Kirschke, S., Bousquet, P., Ciais, P., Saunois, M., Canadell, J. G., Dlugokencky, E. J., Bergamaschi, P., Bergmann, D., Blake, D. R., Bruhwiler, L., Cameron-Smith, P., Castaldi, S., Chevallier, F., Feng, L., Fraser, A., Heimann, M., Hodson, E. L., Houweling, S., Josse, B., … Zeng, G. (2013). Three decades of global methane sources and sinks. *Nature Geoscience*, *6*, 813. https://doi.org/10.1038/ngeo1955. https://www.nature.com/articles/ngeo1955#supplementary-information

Le Mer, J., & Roger, P. (2001). Production, oxidation, emission and consumption of methane by soils: A review. *European Journal of Soil Biology*, *37*(1), 25–50. https://doi.org/10.1016/S1164-5563(01)01067-6

Le Quéré, C., Korsbakken, J. I., Wilson, C., Tosun, J., Andrew, R., Andres, R. J., Canadell, J. G., Jordan, A., Peters, G. P., & van Vuuren, D. P. (2019). Drivers of declining $CO_2$ emissions in 18 developed economies. *Nature Climate Change*, *9*(3), 213–217. https://doi.org/10.1038/s41558-019-0419-7.

Li, Y., Fichot, C. G., Geng, L., Scarratt, M. G., & Xie, H. (2020). The Contribution of Methane Photoproduction to the Oceanic Methane Paradox. *Geophysical Research Letters*, *47*(14), https://doi.org/10.1029/2020GL088362

Maasakkers, J. D., Jacob, D. J., Sulprizio, M. P., Scarpelli, T. R., Nesser, H., Sheng, J.-X., Zhang, Y., Hersher, M., Bloom, A. A., Bowman, K. W., Worden, J. R., Janssens-Maenhout, G., & Parker, R. J. (2019). Global distribution of methane emissions, emission trends, and OH concentrations and trends inferred from an inversion of GOSAT satellite data for 2010–2015. *Atmospheric Chemistry and Physics*, *19*(11), 7859–7881. https://doi.org/10.5194/acp-19-7859-2019

Maasakkers, J. D., Jacob, D. J., Sulprizio, M. P., Scarpelli, T. R., Nesser, H., Sheng, J., Zhang, Y., Lu, X., Bloom, A. A., Bowman, K. W., Worden, J. R., & Parker, R. J. (2021). 2010–2015 North American methane emissions, sectoral contributions, and trends: a high-resolution inversion of GOSAT observations of atmospheric methane. *Atmospheric Chemistry and Physics*, *21*(6), 4339–4356. https://doi.org/10.5194/acp-21-4339-2021

van Marle, M. J. E., Kloster, S., Magi, B. I., Marlon, J. R., Daniau, A.-L., Field, R. D., Arneth, A., Forrest, M., Hantson, S., Kehrwald, N. M., Knorr, W., Lasslop, G., Li, F., Mangeon, S., Yue, C., Kaiser, J. W., & van der Werf, G. R. (2017). Historic global biomass burning emissions for CMIP6 (BB4CMIP) based on merging satellite observations with proxies and fire models (1750–2015). *Geoscientific Model Development*, *10*, 3329–3357. https://doi.org/10.5194/gmd-10-3329-2017

Miller, S. M., Michalak, A. M., Detmers, R. G., Hasekamp, O. P., Bruhwiler, L. M. P., & Schwietzke, S. (2019). China's coal mine methane regulations have not curbed growing emissions. *Nature Communications*, *10*(1), 303. https://doi.org/10.1038/s41467-018-07891-7

Ministry of the Environment, Government of Japan. (2014). *Japan's climate change policies*. Retrieved from https://www.env.go.jp/en/focus/docs/files/20140318-83.pdf

Ministry of the Environment, Government of Japan. (2021). Japan's national greenhouse gas emissions in fiscal year 2019 (Final Figures) [Press release]. Retrieved from https://www.env.go.jp/en/headline/2508.html

Patra, P. K., Krol, M. C., Montzka, S. A., Arnold, T., Atlas, E. L., Lintner, B. R., Stephens, B. B., Xiang, B., Elkins, J. W., Fraser, P. J., Ghosh, A., Hintsa, E. J., Hurst, D. F., Ishijima, K., Krummel, P. B., Miller, B. R., Miyazaki, K., Moore, F. L., Mühle, J., … Young, D. (2014). Observational evidence for interhemispheric hydroxyl-radical parity. *Nature*, *513*(7517), 219–223. https://doi.org/10.1038/nature13721

Pellerin, S., Bamière, L., & Pardon, L. N. C. (2014). *Measures at farm level to reduce greenhouse gas emissions from EU agriculture Note 2*. Retrieved from https://www.europarl.europa.eu/RegData/etudes/note/join/2014/513997/IPOL-AGRI_NT(2014)513997_EN.pdf

Peng, S., Piao, S., Bousquet, P., Ciais, P., Li, B., Lin, X., Tao, S., Wang, Z., Zhang, Y., & Zhou, F. (2016). Inventory of anthropogenic methane emissions in mainland China from 1980 to 2010. *Atmospheric Chemistry and Physics*, *16*(22), 14545–14562. https://doi.org/10.5194/acp-16-14545-2016

Peters, G. P., Andrew, R. M., Canadell, J. G., Fuss, S., Jackson, R. B., Korsbakken, J. I., Le Quéré, C., & Nakicenovic, N. (2017). Key indicators to track current progress and future ambition of the Paris Agreement. *Nature Climate Change*, *7*(2), 118–122. https://doi.org/10.1038/nclimate3202

Petrenko, V. V., Smith, A. M., Schaefer, H., Riedel, K., Brook, E., Baggenstos, D., Harth, C., Hua, Q., Buizert, C., Schilt, A., Fain, X., Mitchell, L., Bauska, T., Orsi, A., Weiss, R. F., & Severinghaus, J. P. (2017). Minimal geological methane emissions during the Younger Dryas-Preboreal abrupt warming event. *Nature*, *548*, 443. https://doi.org/10.1038/nature23316. https://www.nature.com/articles/nature23316#supplementary-information

Poulter, B., Bousquet, P., Canadell, J. G., Ciais, P., Peregon, A., Saunois, M., Arora, V. K., Beerling, D. J., Brovkin, V., Jones, C. D., Joos, F., Gedney, N., Ito, A., Kleinen, T., Koven, C. D., McDonald, K., Melton, J. R., Peng, C., Peng, S., … Zhu, Q. (2017). Global wetland contribution to 2000–2012 atmospheric methane growth rate dynamics. *Environmental Research Letters*, *12*(9), 094013. https://doi.org/10.1088/1748-9326/aa8391

Prigent, C., Jimenez, C., & Bousquet, P. (2020). Satellite-derived global surface water extent and dynamics over the last 25 years (GIEMS-2). *Journal of Geophysical Research: Atmospheres*, *125*(3), e2019JD030711. https://doi.org/10.1029/2019JD030711.

Randerson, J. T., Chen, Y., van der Werf, G. R., Rogers, B. M., & Morton, D. C. (2012). Global burned area and biomass burning emissions from small fires. *Journal of Geophysical Research: Biogeosciences*, *117*(G4), https://doi.org/10.1029/2012JG002128

Roque, B. M., Venegas, M., Kinley, R. D., de Nys, R., Duarte, T. L., Yang, X., & Kebreab, E. (2021). Red seaweed (Asparagopsis taxiformis) supplementation reduces enteric methane by over 80 percent in beef steers. *PLoS ONE*, *16*(3), e0247820. https://doi.org/10.1371/journal.pone.0247820

Saunois, M., Bousquet, P., Poulter, B., Peregon, A., Ciais, P., Canadell, J. G., Dlugokencky, E. J., Etiope, G., Bastviken, D., Houweling, S., Janssens-Maenhout, G., Tubiello, F. N., Castaldi, S., Jackson, R. B., Alexe, M., Arora, V. K., Beerling, D. J., Bergamaschi, P., Blake, D. R., … Zhu, Q. (2016). The global methane budget 2000–2012. *Earth System Science Data*, *8*(2), 697–751. https://doi.org/10.5194/essd-8-697-2016

Saunois, M., Stavert, A. R., Poulter, B., Bousquet, P., Canadell, J. G., Jackson, R. B., Raymond, P. A., Dlugokencky, E. J., Houweling, S., Patra, P. K., Ciais, P., Arora, V. K., Bastviken, D., Bergamaschi, P., Blake, D. R., Brailsford, G., Bruhwiler, L., Carlson, K. M., Carrol, M., … Zhuang, Q. (2020). The global methane budget 2000–2017. *Earth System Science Data*, *12*(3), 1561–1623. https://doi.org/10.5194/essd-12-1561-2020

Sheng, J., Song, S., Zhang, Y., Prinn, R. G., & Janssens-Maenhout, G. (2019). Bottom-up estimates of coal mine methane emissions in China: A gridded inventory, emission factors, and trends.

*Environmental Science and Technology Letters*, *6*(8), 473–478. https://doi.org/10.1021/acs.estlett.9b00294

Thornton, B. F., Wik, M., & Crill, P. M. (2016). Double-counting challenges the accuracy of high-latitude methane inventories. *Geophysical Research Letters*, *43*(24), 12,569–512,577. https://doi.org/10.1002/2016GL071772

Tian, Y., Zhang, J.-B., & He, Y.-Y. (2014). Research on spatial-temporal characteristics and driving factor of agricultural carbon emissions in China. *Journal of Integrative Agriculture*, *13*(6), 1393–1403. https://doi.org/10.1016/S2095-3119(13)60624-3

United Nations Environment Programme, & Climate and Clean Air Coalition. (2021). *Global methane assessment: Benefits and costs of mitigating methane emissions*. Retrieved from Nairobi: https://www.ccacoalition.org/en/resources/global-methane-assessment-full-report

USEPA (2012). *Global anthropogenic non-$CO_2$ greenhouse gas emissions: 1990–2030*. Retrieved from Washington, DC.

van der Werf, G. R., Randerson, J. T., Giglio, L., van Leeuwen, T. T., Chen, Y., Rogers, B. M., Mu, M., van Marle, M. J. E., Morton, D. C., Collatz, G. J., Yokelson, R. J., & Kasibhatla, P. S. (2017). Global fire emissions estimates during 1997–2016. *Earth System Science Data*, *9*(2), 697–720. https://doi.org/10.5194/essd-9-697-2017

Vergé, X. P. C., De Kimpe, C., & Desjardins, R. L. (2007). Agricultural production, greenhouse gas emissions and mitigation potential. *Agricultural and Forest Meteorology*, *142*(2), 255–269. https://doi.org/10.1016/j.agrformet.2006.06.011

Wiedinmyer, C., Akagi, S. K., Yokelson, R. J., Emmons, L. K., Al-Saadi, J. A., Orlando, J. J., & Soja, A. J. (2011). The Fire INventory from NCAR (FINN): A high resolution global model to estimate the emissions from open burning. *Geoscientific Model Development*, *4*(3), 625–641. https://doi.org/10.5194/gmd-4-625-2011

Williams, J. P., Regehr, A., & Kang, M. (2021). Methane emissions from abandoned oil and gas wells in Canada and the United States. *Environmental Science and Technology*, *55*(1), 563–570. https://doi.org/10.1021/acs.est.0c04265.

Yin, Y. I., Chevallier, F., Ciais, P., Bousquet, P., Saunois, M., Zheng, B. O., Worden, J., Bloom, A. A., Parker, R. J., Jacob, D. J., Dlugokencky, E. J., & Frankenberg, C. (2021). Accelerating methane growth rate from 2010 to 2017: Leading contributions from the tropics and East Asia. *Atmospheric Chemistry and Physics*, *21*(16), 12631–12647. https://doi.org/10.5194/acp-21-12631-2021

Zhang, B., & Chen, G. Q. (2010). Methane emissions by Chinese economy: Inventory and embodiment analysis. *Energy Policy*, *38*(8), 4304–4316. https://doi.org/10.1016/j.enpol.2010.03.059

Zhang, Y., Jacob, D. J., Lu, X., Maasakkers, J. D., Scarpelli, T. R., Sheng, J. X., & Boesch, H. (2020). Attribution of the accelerating increase in atmospheric methane during 2010–2018 by inverse analysis of GOSAT observations. *Atmospheric Chemistry and Physics Discussion*, *2020*, 1–42. https://doi.org/10.5194/acp-2020-964

Zhang, Z., Fluet-Chouinard, E., Jensen, K., McDonald, K., Hugelius, G., Gumbricht, T., Carroll, M., Prigent, C., Bartsch, A., & Poulter, B. (2021). Development of the global dataset of wetland area and dynamics for methane modeling (WAD2M). *Earth System Science Data*, *13*(5), 2001–2023. https://doi.org/10.5194/essd-13-2001-2021

Zhang, Z., Zimmermann, N. E., Calle, L., Hurtt, G., Chatterjee, A., & Poulter, B. (2018). Enhanced response of global wetland methane emissions to the 2015–2016 El Nino-Southern Oscillation event. *Environmental Research Letters*, *13*(7), 13. https://doi.org/10.1088/1748-9326/aac939

Zhao, Y., Saunois, M., Bousquet, P., Lin, X., Berchet, A., Hegglin, M. I., Canadell, J. G., Jackson, R. B., Hauglustaine, D. A., Szopa, S., Stavert, A. R., Abraham, N. L., Archibald, A. T., Bekki, S., Deushi, M., Jöckel, P., Josse, B., Kinnison, D., Kirner, O., … Zheng, B. O. (2019). Inter-model comparison of global hydroxyl radical (OH) distributions and their impact on atmospheric methane over the 2000–2016 period. *Atmospheric Chemistry and Physics*, *19*(21), 13701–13723. https://doi.org/10.5194/acp-19-13701-2019

## SUPPORTING INFORMATION

Additional supporting information may be found in the online version of the article at the publisher's website.

**How to cite this article:** Stavert, A. R., Saunois, M., Canadell, J. G., Poulter, B., Jackson, R. B., Regnier, P., Lauerwald, R., Raymond, P. A., Allen, G. H., Patra, P. K., Bergamaschi, P., Bousquet, P., Chandra, N., Ciais, P., Gustafson, A., Ishizawa, M., Ito, A., Kleinen, T., Maksyutov, S., … Zhuang, Q. (2022). Regional trends and drivers of the global methane budget. *Global Change Biology*, 28, 182–200. https://doi.org/10.1111/gcb.15901